Author/s:
Zhang, J;Hoedt, EC;Liu, Q;Berendsen, E;Teh, JJ;Hamilton, A;O' Brien, AW;Ching, JYL;Wei, H;Yang, K;Xu, Z;Wong, SH;Mak, JWY;Sung, JJY;Morrison, M;Yu, J;Kamm, MA;Ng, SC

Title:
Elucidation of Proteus mirabilis as a Key Bacterium in Crohn's Disease Inflammation

Date:
2021-01-01

Citation:
Zhang, J., Hoedt, E. C., Liu, Q., Berendsen, E., Teh, J. J., Hamilton, A., O' Brien, A. W., Ching, J. Y. L., Wei, H., Yang, K., Xu, Z., Wong, S. H., Mak, J. W. Y., Sung, J. J. Y., Morrison, M., Yu, J., Kamm, M. A. & Ng, S. C. (2021). Elucidation of Proteus mirabilis as a Key Bacterium in Crohn's Disease Inflammation. Gastroenterology, 160 (1), pp.317-330.e11. https://doi.org/10.1053/j.gastro.2020.09.036.

Persistent Link:
https://hdl.handle.net/11343/274475

Gastroenterology 2021;160:317–330

Elucidation of *Proteus mirabilis* as a Key Bacterium in Crohn's Disease Inflammation

Jingwan Zhang,[1] Emily C. Hoedt,[2,3] Qin Liu,[1] Erwin Berendsen,[2] Jing Jie Teh,[2] Amy Hamilton,[4,5] Amy Wilson O' Brien,[4,5] Jessica Y. L. Ching,[1] Hong Wei,[6] Keli Yang,[1] Zhilu Xu,[1] Sunny H. Wong,[1,7] Joyce W. Y. Mak,[1] Joseph J. Y. Sung,[1] Mark Morrison,[2] Jun Yu,[1,7] Michael A. Kamm,[4,5] and Siew C. Ng[1,7]

[1]Department of Medicine and Therapeutics, Institute of Digestive Disease, State Key Laboratory of Digestive Diseases, Li Ka Shing Institute of Health Science, The Chinese University of Hong Kong, Hong Kong, China; [2]The University of Queensland Diamantina Institute, Faculty of Medicine, Brisbane, Australia; [3]APC Microbiome Ireland, University College Cork, Cork, Ireland; [4]Department of Gastroenterology, St Vincent's Hospital, Melbourne, Australia; [5]Department of Medicine, The University of Melbourne, Melbourne, Australia; [6]Department of Laboratory Animal Science at the Third Military Medical University in Chongqing, China; and [7]Center for Gut Microbiota Research, Department of Medicine and Therapeutics, The Chinese University of Hong Kong, Hong Kong, China

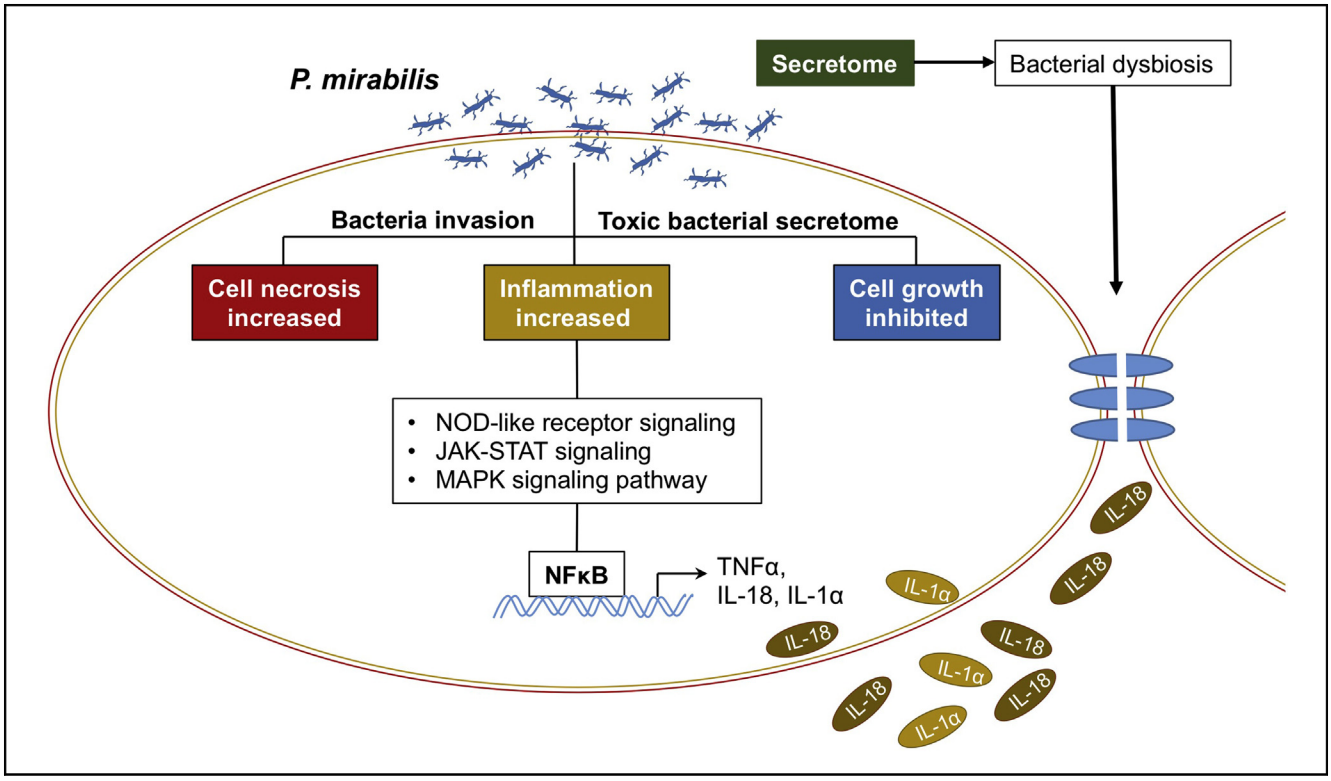

BACKGROUND & AIMS: *Proteus* spp, Gram-negative facultative anaerobic bacilli, have recently been associated with Crohn's disease (CD) recurrence after intestinal resection. We investigated the genomic and functional role of *Proteus* as a gut pathogen in CD. **METHODS:** *Proteus* spp abundance was assessed by *ure* gene–specific polymerase chain in 54 pairs of fecal samples and 101 intestinal biopsies from patients with CD and healthy controls. The adherence, invasion, and intracellular presence of 2 distinct isolates of *Proteus mirabilis* in epithelial cells were evaluated using immunofluorescence and electron microscopy. Intracellular gene expression profiles and regulated pathways were analyzed by RNA sequencing and KEGG pathway analysis. Biologic functions of 2 isolates of *P mirabilis* were determined by in vitro cell culture, and in vivo using conventional mice and germ-free mice. **RESULTS:** *Proteus* spp were significantly more prevalent and abundant in fecal samples and colonic tissue of patients with CD than controls. A greater abundance of the genus *Fusobacterium* and a lesser abundance of the genus *Faecalibacterium* were seen in patients with CD with a high *Proteus* spp abundance. All 24 *Proteus* monoclones isolated from patients with CD belonged to members of *P mirabilis* lineages and 2 isolates, recovered from stool or mucosa, were used in further studies. Mice gavaged with either *P mirabilis* strain had more severe colonic inflammation.

Co-culture of the isolates with epithelial cell lines showed bacterial adherence, invasion, increased production of pro-inflammatory cytokines IL-18 and IL-1α, and cell necrosis. Both isolates induced key pro-inflammatory pathways, including NOD-like receptor signaling, Jak-STAT signaling, and MAPK signaling, and induced pro-inflammatory genes and activated inflammation-related pathways in gnotobiotic mice. **CONCLUSIONS:** *P mirabilis* in the gut is associated with CD and can induce inflammation in cells and animal models of colitis. *P mirabilis* can act as a pathobiont and play a crucial role in the pathogenesis of CD.

Keywords: P mirabilis; Crohn's Disease; Inflammation; Pathogen.

WHAT YOU NEED TO KNOW

BACKGROUD AND CONTEXT

Proteus spp., Gram-negative facultative anaerobic bacilli, have recently been associated with Crohn's disease (CD) recurrence after intestinal resection. The authors investigated the genomic and functional role of *Proteus* as a gut pathogen in CD.

NEW FINDINGS

P mirabilis promotes CD progression by inducing intestinal dysbiosis, activating intracellular pro-inflammatory pathways and promoting secretion of inflammatory cytokines. *P. mirabilis* thus play a crucial role in pathogenesis of CD.

LIMITATIONS

The direct interaction of *P. mirabilis* and its receptors on colon epithelial cells needs further investigation.

IMPACT

P mirabilis may regarded as a diagnostic and therapeutic target to improve patient recovery and remission.

The pathogenesis of Crohn's disease (CD) relates to a dysregulated immune response to the intestinal microbiota, sometimes in genetically predisposed individuals.[1] Changes in composition of the intestinal bacterial community and reduced microbial richness and diversity have been observed in CD.[2,3] Specifically, reduced *Firmicutes,* principally *Clostridia,* and increased levels of *Proteobacteria* have been reported in patients with CD.[4–6]

The recent identification of *Proteus* spp as a potential pathogen in CD recurrence after intestinal resection prompted us to further examine its potential role as a gut pathogen.[7,8] Our group previously reported that the combination of detectable *Proteus* spp with reduced relative abundance of *Faecalibacterium* spp (<0.1%) in post-operative ileal biopsies was associated with a 14-fold increased risk of CD recurrence. Furthermore, the presence of *Proteus* spp, absence of *Faecalibacterium prausnitzii,* and a positive smoking history were predictive for disease recurrence after resection in CD.[8] A recent study showed by metagenome sequencing that urease genes were present in higher numbers in patients with CD, indicative of a metabolic shift in nitrogen metabolism in the microbial population. In addition, a recombinant *Escherichia coli* strain carrying a urease operon from *P mirabilis* shifted the microbial population in a mouse model.[9]

Proteus spp are Gram-negative bacilli and facultative anaerobes, assigned to the *Gammaproteobacteria*, and within this bacterial lineage to the *Morganellaceae* (fam. nov), which also includes *Morganella* and *Providencia* spp.[10] Members of these genera are commonly implicated in urinary tract infections[11] as well as cholangitis, liver abscess, and sepsis.[12–14] As such, *Proteus* spp can cause infection as a pathogen and trigger systemic inflammation.[15,16] Until recently, *Proteus* spp have not been explored in the gastrointestinal tract, in part due to its low abundance precluding its detection via microbiome sequencing and bioinformatics. No studies have focused on the role of *Proteus* spp at the mucosa level. It is also unclear whether *Proteus* spp enrichment in patients with CD represents an indirect association, or whether *Proteus* spp functionally contributes to CD inflammation, progression and disease recurrence.

To understand the pathogenic role of *Proteus* spp, we selectively isolated strains of this bacterium from stool and mucosal tissue samples and investigated their characteristics at the molecular, biochemical, and microbiologic levels. We also investigated their functional significance in animal models. To our knowledge, this is the first investigation that illustrates a novel and important mechanism of *P mirabilis*–mediated inflammation in the development of CD and highlights the potential of therapeutically targeting *P mirabilis* and related bacteria in patients with CD.

Material and Methods

Human Samples

Stool samples were collected from 54 patients with CD and 54 healthy controls and stored at –80°C. A total of 114 colonic biopsies (45 noninflamed CD, 29 inflamed CD, and 40 healthy controls) were obtained from the terminal ileum and right colon of 107 subjects undergoing colonoscopy, including 67 patients with CD and 40 controls at the Prince of Wales Hospital, the Chinese University of Hong Kong. The samples were snap-frozen in cryovials immediately after colonoscopy and stored at –80°C until DNA extraction.

Patients were included if they were 18 years or older and had a diagnosis of CD defined by endoscopy, radiology, and histology; were on stable medication; and consented to biopsies during colonoscopy. Patients were excluded if they had infection with an enteric pathogen; had short bowel syndrome; or had significant hepatic, renal, endocrine, respiratory,

Abbreviations used in this paper: **CD, Crohn's disease; cfu, colony-forming units; DSS, dextran sulfate sodium; qPCR, quantitative polymerase chain reaction.**

Most current article

0016-5085
https://doi.org/10.1053/j.gastro.2020.09.036

neurologic, or cardiovascular disease. Healthy individuals who underwent screening colonoscopy and were found to have a normal macroscopic colon and no evidence of microscopic inflammation after colonoscopy were included as controls. Individuals who had a first- or second-degree relative with inflammatory bowel disease were excluded as controls. Clinical and pathologic characteristics of patients are shown in Supplementary Table 1. Patient metadata are provided in Supplementary Table 2. Written informed consents were obtained from all subjects and the study protocol was approved by the Ethics Committee of the Chinese University of Hong (2017.495 and CRE 2014.026).

Isolation of Proteus *spp From Stool and Biopsy and Genome Sequencing*

Based on a positive urease polymerase chain reaction (PCR), 4 stool samples and 1 colonic biopsy sample from patients with CD were selected for targeted isolation of *Proteus* spp. Samples were treated using 0.1% (v/v) Triton, followed by serial dilutions in saline. Dilutions were plated on Drigalski lactose agar, followed by incubation at 37°C overnight. Colonies were selected based on a swarming phenotype and the inability to ferment lactose. PCR was performed on selected colonies with *ureR* and *ureC* primers. Detailed methods relating to microbial genome sequencing, assembly, and analyses are provided in the Supplementary Methods.

Animal Experiments

To explore the role of *P mirabilis* in pathogenesis of colonic inflammation in vivo, male C57BL/6 mice (6 weeks of age) were treated with a cocktail of broad-spectrum antibiotics, including ampicillin (0.2 g/L), vancomycin (0.1 g/L), neomycin (0.2 g/L), and metronidazole (0.2 g/L), in their drinking water for 5 days before a single-dose treatment of 1.5% dextran sulfate sodium (DSS) in autoclaved water to induce colitis. Two days later, the mice were gavaged with 1×10^9 colony-forming units (cfu) of either *P mirabilis* strain W5 or strain W19 for 3 consecutive days. As a control, similarly treated mice received a gavage of *E coli* MG1655, and the mice were observed for 10 days. To further explore the role of these 2 *P mirabilis* strains in gut dysbiosis, we designed 2 other types of mouse models. In the first model, mice were treated with low-dose DSS (0.5%) in drinking water for 3 weeks, followed by 1 week with normal water to minimize the pathogenic effect. *P mirabilis* or *E coli* MG1655 was inoculated to the mice once per day for 3 continuous days after 2 days treatment with DSS. In the second model, the mice were administrated either 1×10^9 cfu of *P mirabilis* or *E coli* MG1655 every 3 days for 4 weeks. All animal studies were performed in accordance with guidelines approved by the Animal Experimentation Ethics Committee of The Chinese University of Hong Kong.

The germ-free C57BL/6 mice were bred at the Department of Laboratory Animal Science at the Third Military Medical University in Chongqing, China. Adult mice (6 weeks of age) were divided into 4 groups and were treated with either 1×10^9 cfu of *P mirabilis* or *E coli* MG1655 for 2 weeks. The oral gavage of bacteria was performed for 2 continuous days from the beginning. All mice were sacrificed 2 weeks after the second gavage.

Electron Microscopy

Approximately 1×10^6 normal cells were grown in a 6-well plate co-cultured with bacteria for 2 hours (multiplicity of infection = 10) and then fixed using 2.5% glutaraldehyde. Fixed cell samples were further fixed using 1% osmium tetroxide, followed by dehydration with an increasing concentration gradient of ethanol and propylene oxide. Samples were then embedded, cut into 50-nm sections, and stained with 3% uranyl acetate and lead citrate. The sections were observed with Philips CM100 Transmission Electron Microscope (FEI; Philips Healthcare, Amsterdam, The Netherlands).

Transcriptome Shotgun Sequencing and Data Analysis

Total RNA from epithelial cells were isolated using TRIzol reagent (Life Technologies, Invitrogen, Carlsbad, CA), quantified using a NanoDrop2000 (Thermo-Fisher, Waltham, MA). RNA sequencing was performed by Beijing Novogene Technology (Beijing, China). Before differential gene expression analysis, for each sequenced library, the read counts were adjusted by edgeR program package through 1 scaling normalized factor. Differential expression analysis of 2 conditions was performed using the edgeR R package, version 3.16.5. *P* values were adjusted using the Benjamini & Hochberg method. Corrected *P* value of .05 and absolute fold-change of 2 were set as the threshold for significantly differential expression. ClusterProfiler R package was used to test the statistical enrichment of differential expression genes in KEGG pathways.

Data Analysis

Multiple group comparisons were made by Kruskal–Wallis test or 1-way analysis of variance. Blocked Wilcoxon rank-sum test was used to evaluate the abundance of *Proteus* spp in CD and normal colon tissue. $P < .05$ was considered statistically significant. Data are expressed as mean ± SD from 3 independent experiments. All tests were performed using GraphPad Prism (GraphPad, La Jolla, CA) or SPSS (IBM Corp, Armonk, NY) software.

Results

Proteus *spp Are Enriched in stool and Colonic Mucosa of Subjects With Crohn's Disease*

We examined the prevalence of *Proteus* spp in 108 stool samples from 54 patients with CD and 54 controls using PCR targeting the *ureC* and/or *ureR* genes. The prevalence of *Proteus* spp presence was higher in CD than controls (18.5% vs 5.6%; $P < 0.05$) (Figure 1*A* and Supplementary Figure 1). We also examined the abundance of *Proteus* spp in 114 biopsy samples from 67 patients with CD and 40 controls by quantitative PCR (qPCR). *Proteus* spp abundance were also significantly higher in CD compared with control tissues (noninflamed, $P < .01$; inflamed, $P < .001$) (Figure 1*B*). The relative abundance of *Proteus* spp was higher in biopsies collected from terminal ileum and right colon of patients with CD compared with their corresponding healthy controls, respectively ($P < .001$ and $P < .05$) (Supplementary Figure 1*B*). Within patients with CD, abundance of *Proteus* spp in terminal ileum and the right colon showed no

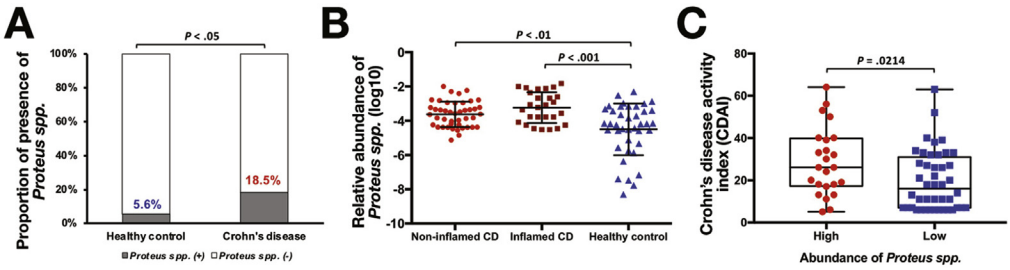

Figure 1. *Proteus* spp are enriched in both stool and mucosal tissue samples from patients with CD compared with healthy controls. (*A*) The prevalence of *Proteus* spp in stool samples from normal subjects (5.6%) is much lower than those from patients with CD (18.5%). (*B*) The relative abundance of *Proteus* spp is similar in noninflamed and inflamed CD mucosal tissues and higher than that observed in healthy controls. (*C*) Patients with CD with relatively high *Proteus* spp also have more severe disease, as measured by Crohn's diseases activity index scores.

significant difference ($P = .0614$). However, a greater relative abundance of *Proteus* spp was observed with biopsies from inflamed tissue compared with patient-paired biopsy samples from noninflamed regions (n = 7 patients; Supplementary Figure 1*C*) ($P < .05$).

Based on the mean abundance of *Proteus* spp in mucosal tissues determined by qPCR, the CD patient samples were grouped as high *Proteus* or low *Proteus*. The high *Proteus* patient group had significantly higher Crohn's disease activity index scores compared with the low *Proteus* group ($P < .05$; Figure 1*C*), suggesting that those patients with a greater relative abundance of *Proteus* spp might be afflicted with more severe CD activity.

Patients in the High Proteus *Group Have Reduced Bacterial Diversity and Differences in Their Mucosa-Associated Microbiota Profiles in Crohn's Disease*

The abundance of *Proteus* in each mucosal sample from patients with CD and normal individuals is shown in Supplementary Figure 2*A*. The *Proteus* prevalence in mucosal samples was approximately 65%—24 samples with detectable *Proteus* spp (12 in high *Proteus* group and 12 in low *Proteus* group) and 14 samples with no detectable *Proteus* spp. Bacterial α- and β-diversity identified significant differences between those patients with CD with a high *Proteus* abundance (n = 12) compared with those assigned to the low *Proteus* group (n = 26) at genus level (Figure 2*A* and Supplementary Figure 2*B*). The distribution of the top 10 compositional taxa are shown in Figure 2*B*. Notably, *Fusobacterium* was more abundant and *Faecalibacterium* was reduced in the high *Proteus* group (both, $P < .05$) (Figure 2*B*). Based on bacteria heatmap analysis, bacterial composition and abundance in the low *Proteus* CD subjects were more similar to those of controls (Figure 2*C*). The similar observations were also found at species level (Supplementary Figure 2*C*–*E*). To compare the bacterial community in high vs low *Proteus* groups in CD, supervised comparisons by linear discriminant analysis effect size (linear discriminant analysis > 2.0) were performed at the species level. The abundance of *Gemmiger formicilis, Blauria obeum, Dorea formicigenerans, Coprococcus catus, Bacillus coagulans, Lactobacillus helveticus, Coprococcus eutactus, Rahnella aquatilis, Blautia producta, Desulfovibrio D168, Ruminococcus albus, Ruminococcus callidus, Acinetobacter rhizosphaerae*, and *Bulleidia moorei* were found to be significantly lower in samples harboring high *Proteus* than those with low *Proteus*, while *Lactobacillus ruminis, Clostridium posteurianum, Sphingomonas yabuuchiae, Kocuria palustris, Methylobacterium adhaesivum*, and *Serratia marcescens* were significantly higher in samples with high *Proteus* than in those with low *Proteus* abundance (Figure 2*D*). As shown in Figure 2*E*, *Proteus* spp was negatively correlated with taxa enriched in low *Proteus* samples, and positively associated with those bacterial taxa abundant in the high *Proteus* group. Interestingly, members of *Bacteroidetes* and *Fusobacterium* were more likely to form strong co-occurring relationships with one another in the high *Proteus* CD patient group (Figure 2*F*), and such findings were not seen in control samples.

All of the Clinical Isolates Recovered From the Crohn's Disease Samples Are Proteus mirabilis *but There Are Strain-Specific Differences Between Stool and Mucosa-Associated Isolates*

Twenty-five candidate isolates of *Proteus* spp were recovered from 4 stool samples (18 isolates) and 1 biopsy sample (7 isolates) from patients with CD and of these 24 of 25 were confirmed by PCR to be *ureC/ureR*-positive (Figure 3*A*). The phylogenetic tree based on the 16S ribosomal RNA gene sequences of our strains and 33 other *P mirabilis* isolates (Supplementary Table 3) is shown in Figure 3*B*. Most of the isolates recovered here (22 of 24) were most closely related to *P mirabilis* isolates from the urinary tract, principally from subjects in the United States (n = 11), China and Taiwan (n = 2 each) and Poland (n = 1).[17] This cluster also contains 2 strains from stool samples from a Chinese (GCF_000313255.1) and a Swedish subject (GCF_003194305.1).[18,19] Interestingly, the remaining 2 isolates, both recovered from the patient biopsy sample of patient W19, were assigned to a distinct branch within the *P mirabilis* lineage, along with an isolate recovered from a stool sample as part of the National Institutes of Health Human Microbiome Project.

The average nucleotide identity scores produced from the core gene orthologs of the 57 genomes all exceed 96%,

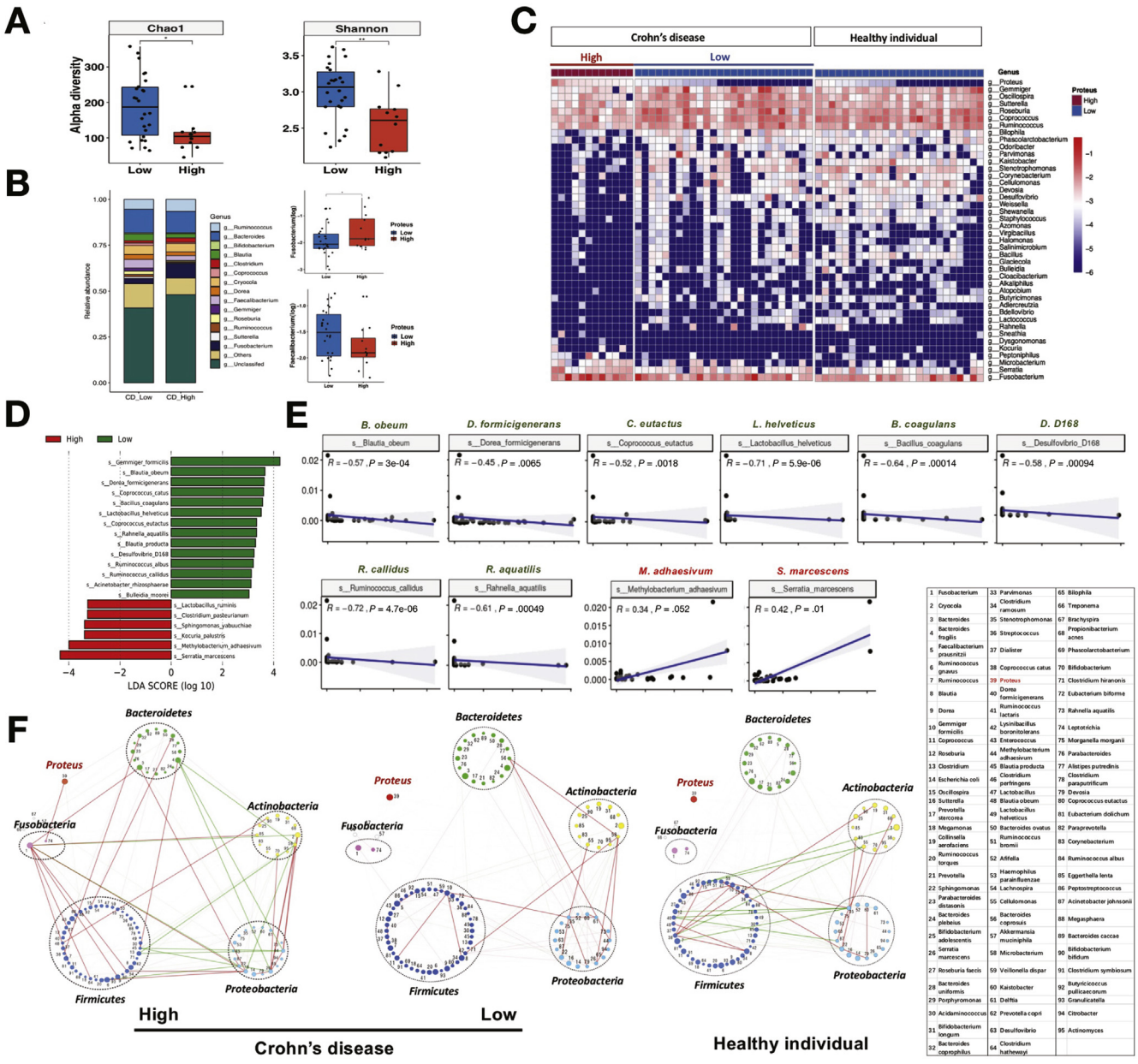

Figure 2. The mucosa-associated microbiota profiles of patients with CD with a high relative abundance of *Proteus* spp differ from patients with CD with low *Proteus* spp, as well as healthy controls. (*A*) Chao1 and Shannon diversity scores are reduced for mucosa-associated microbial communities containing high levels of *Proteus* spp at genus level. (*B*) Genus-level *histograms* show these differences extend to the top 10 dominant genera and particularly the relative abundances of *Fusobacterium* spp increase and *Faecalibacterium* spp decrease in patients with CD with high *Proteus* spp. (*C*) The genus-level *heatmaps* show the bacterial profiles from the high and low *Proteus* spp CD patient groups are clearly different, and the profiles from the low *Proteus* spp group are more similar to those from healthy control subjects. (*D*) Linear discriminant analysis effect size at the species-level also shows the bacterial communities with low *Proteus* spp group can be discriminated from the high *Proteus* spp. (*E*) *Correlation plots* of those bacterial taxa with significant positive or negative correlations with the relative abundance of *Proteus* spp in patients with CD. (*F*) Network analysis of bacterial taxa showing co-association and co-exclusion relationships in communities produced from normal and CD biopsies and differentiated between high and low *Proteus* spp abundance. The correlation coefficients were estimated and corrected for compositional effects using the SparCC algorithm, and the numerical annotation of the bacterial taxa is also provided.

further confirming that all of the isolates belonged to the *P mirabilis* lineage (Figure 3*C*). The summary table of KEGG-based annotations is shown in Figure 3*D*, and all of the new isolates from this study possess the *ure* operon, *zapA* (metalloprotease) and *hpmA* (hemolysin) genes. Furthermore, the Mauve alignments of the *P mirabilis* W5 and W19 genomes, as a representative of each cluster, with *P mirabilis* HI4320, showed extensive synteny among all 3

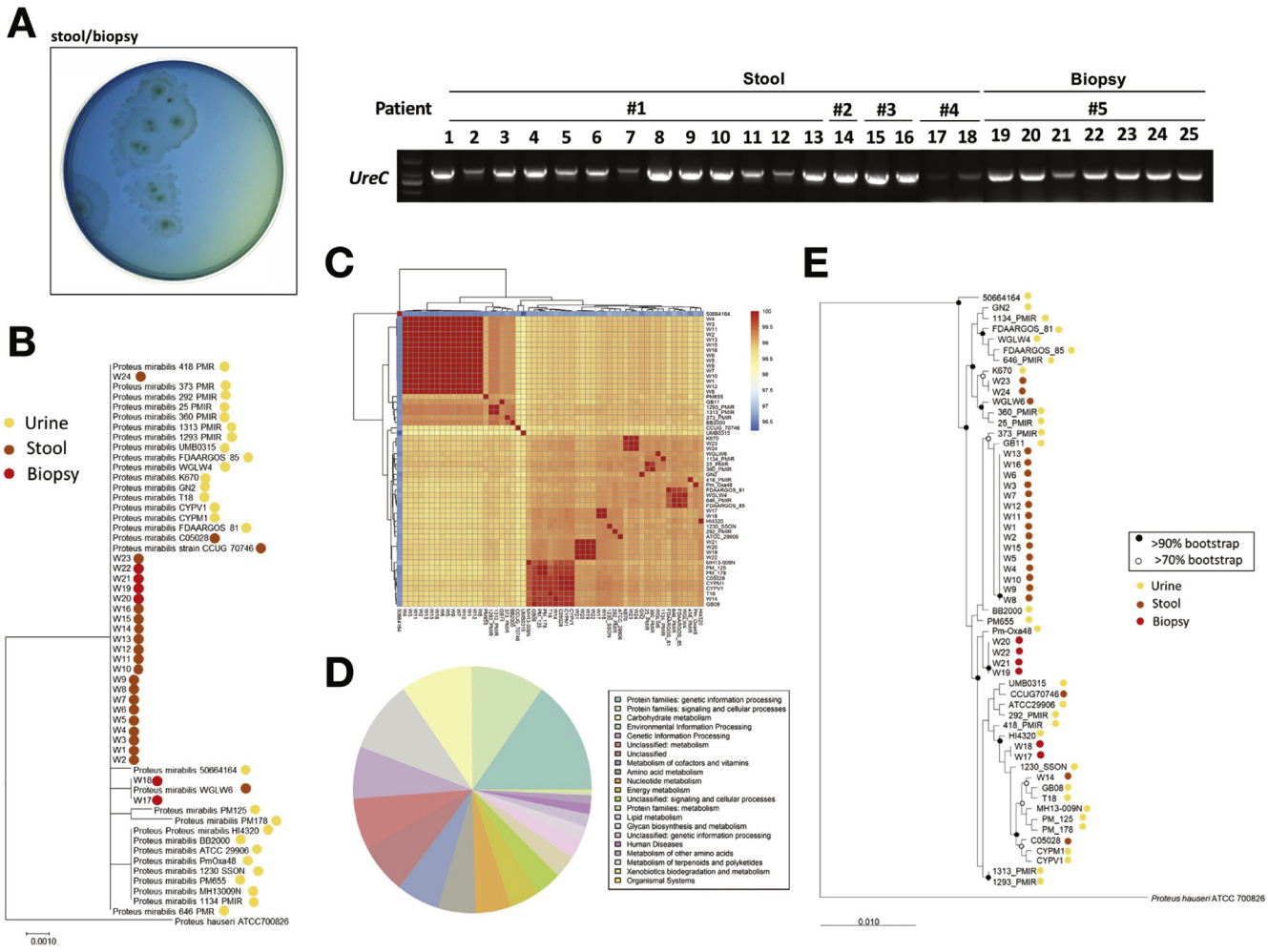

Figure 3. All candidate *Proteus* spp isolated from the CD fecal and mucosal samples of this patient group are *P mirabilis*. (*A*) Representative colony morphology of a candidate *Proteus* sp clinical isolate on agar selective medium, with secondary confirmation provided by *ureC*-specific PCR. (*B*) Phylogenetic analysis of 16S ribosomal RNA gene sequences shows all the clinical isolates produced from this study are assigned to the *P mirabilis* lineage, and closely affiliated with 33 other *P mirabilis* strains described inSupplementary Table 3. Node *colors* depict the source of each strain from either urine (*yellow*), stool (*brown*), or biopsy samples (*red*). (*C*) The average nucleotide identity (ANI) matrix for the 57 *P mirabilis* genomes representing the 24 clinical isolated from Hong Kong patients with CD and the 33 additional *P mirabilis* genomes deposited in the National Center for Biotechnology Information (NCBI) databases. (*D*) The relative distribution of orthologs assigned to the major KEGG categories for the core genome produced from the 24 Hong Kong clinical isolates and 33 genomes of *P mirabilis* deposited in NCBI. (*E*) The genome-based phylogenetic tree of the isolate and NCBI representative genomes constructed from 120 marker genes using Genome Taxonomy DataBase. Node *colors* depict the source of each strain, from either urine (*yellow*), stool (*brown*), or biopsy samples (*red*).

genomes (Supplementary Figure 3*A*) and the virulence genes predicted by RAST were highly similar between strains from stool and mucosa (Supplementary Figure 3*B*). The core and pangenome plots of the *P mirabilis* genomes, and a detailed inventory of KEGG-based annotations, are provided in Supplementary Figure 3*C* andSupplementary Table 4, respectively.

Despite these similarities, the whole genome phylogeny of these isolates predicted using the Genome Taxonomy Database workflow maintained their distinct placement across 2 clusters, as was inferred from the 16S ribosomal RNA gene analysis (Figure 3*E*). The isolates from stool most closely affiliated with the urinary tract isolates and were clearly separated from 2 of the isolates recovered from the CD patient biopsy sample. The *P mirabilis* core genome based on our analyses encodes 46 fimbriae-associated genes; however, the genome from *P mirabilis* strain W5 (stool) possessed fewer fimbriae-associated genes (n = 107) compared with strain W19 (mucosa, n = 119) (Supplementary Table 5). We next determined the shared and singleton gene counts for the genomes of these 2 isolates by reciprocal BLASTp analysis of the EDGAR-based predictions of the protein-coding genes from each genome. The 2 strains shared 3147 genes, and the singleton count was 295 and 231 genes for stool strains (W5) and mucosa strains (W19), respectively. The resulting KEGG-based

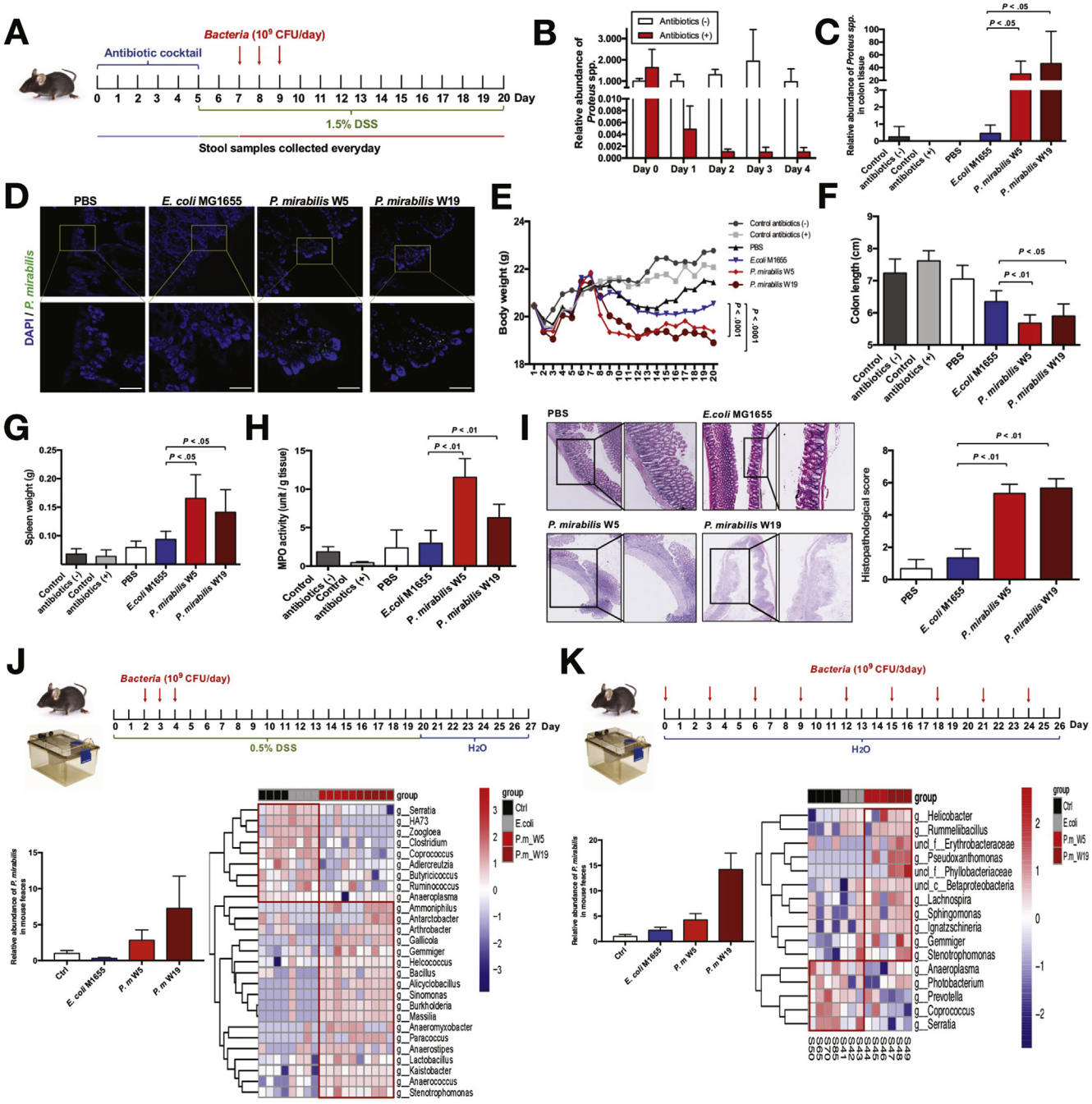

Figure 4. *Proteus* spp promote colonic inflammation and mucosal bacterial dysbiosis in mice. (*A*) *Schematic diagram* showing the experimental design and timeline of mouse models. (*B*) The level of *P mirabilis* in stool samples of mice during the antibiotic treatment period by qPCR. (*C*) The level of *P mirabilis* in colonic samples of mice was checked by qPCR. (*D*) Fluorescence in situ hybridization detection of *P mirabilis* in colonic tissues using an Alexa Fluor 488–conjugated *P mirabilis*–specific probe (*green*). Scale bars: 50 μm. (*E*) Body weight, (*F*) colon length, and (*G*) spleen weight change of mice were measured. (*H*) *Bar graph* for the myeloperoxidase (MPO) activity in control, *E coli* M1655, and *P mirabilis*–inoculated mice. (*I*) *P mirabilis* promoted colonic inflammation. Representative histologic images of colon tissues of mice by H&E staining and statistical analysis of colon samples according to the histologic score. (*J*) 0.5% DSS mouse model. (*K*) Chemical-free mouse model. The level of *P mirabilis* in fecal samples of mice was checked by qPCR. *Taxonomic heatmap* using Bray-Curtis Dissimilarity index distance, combined with average (unweighted pair-group method with arithmetic means) clustering for the most statistically significant operational taxonomic units between control and *P mirabilis*–infected mucosal samples of the mice. *Red* and *blue* represent high and low abundance, respectively.

annotation of these singleton genes was small (approximately 8%,Supplementary Table 6). The annotated singleton genes present in the *P mirabilis* strain W5 genome encode for bacteriophage-related proteins and their assembly, and multiple copies of genes encoding "putative large exoprotein involved in heme utilization or adhesion of

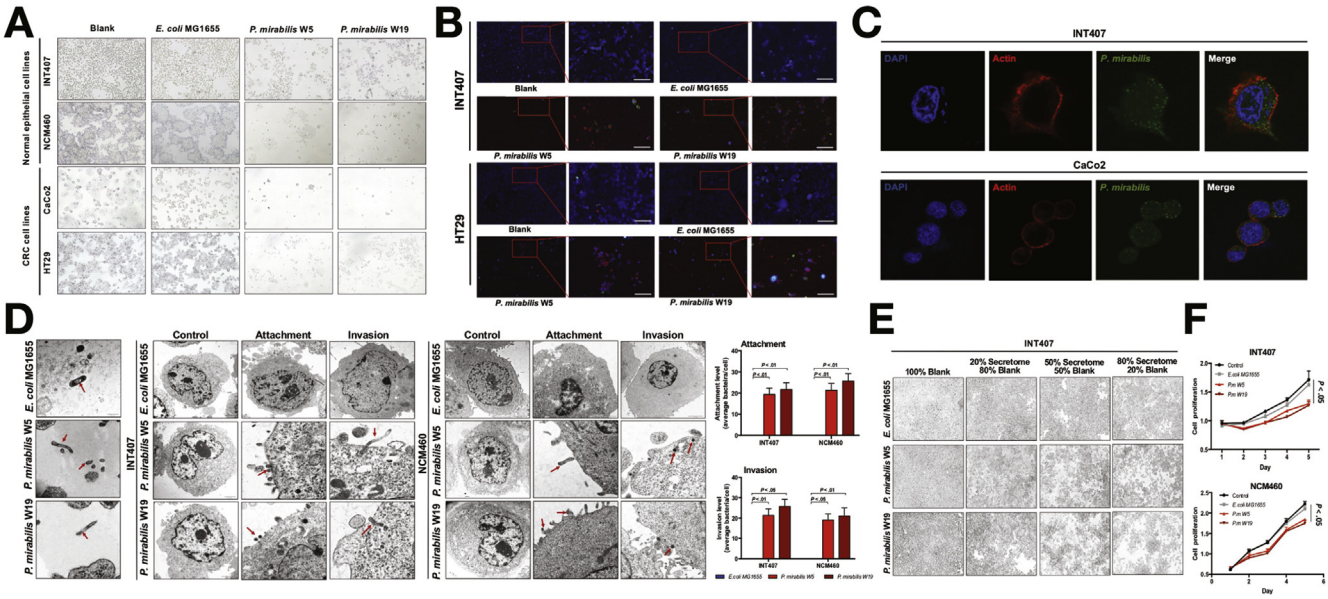

Figure 5. *Proteus* sp induced epithelial cell necrosis through cell cytoplasm invasion. Secretome of *Proteus* sp can inhibit cell proliferation. (*A*) Presentative *photos* for morphology for cells co-cultured with *E coli* MG1655 and *P mirabilis* W5 and W19. (*B*) Confocal immunofluorescence analysis of normal, apoptotic and necrotic cells with *blue*, *green,* and *red* signals. Scale bars: 50 μm. (*C*) INT407 and CaCo2 cells were infected for 3 hours with *P mirabilis* strains (*green*). Cell membrane was stained with Actin (*red*), and nucleus was stained with 4′,6-diamidino-2-phenylindole (*blue*). Cells were imaged using confocal microscopy. (*D*) Representative transmission electron microscopy images of *P mirabilis* attaching and invading into normal colon INT407 and NCM460 cells. *E coli* MG1655 was used as the negative control. *Red arrows* indicate *P mirabilis*. (*E*) Representative images of morphology of INT407 cells cultured with different concentration of secretome collected from *P mirabilis*. (*F*) Cell viability was measured by MTT assay at 0, 1, 2, 3, and 4 days after adding the conditional proteins into the medium. Data are means ± SEM of at least 3 independent experiments (n = 3) performed in duplicate.

ShlA/HecA/FhaA family"; and the mucosa W19 genome included fimbrial and adhesion proteins and a smaller number of bacteriophage-related proteins. These data suggest that the *P mirabilis* isolates from our stool and biopsy tissue samples are not clonal, and *P mirabilis* strains W5 and W19 each represent a distinct cluster within our *P mirabilis* collection. W19, which was isolated from a tissue biopsy of a patient with CD, showed more fimbrial and adhesion proteins than W5 that was isolated from the stool.

Proteus mirabilis *Strains Promote Colonic Inflammation in Mice*

We next assessed whether the chosen *P mirabilis* strains could induce gut inflammation in conventional mice. We established depletion of natural gut flora in mice by treating them with the antibiotic cocktail for 5 days (Figure 4*A*). Stool samples of mice treated with antibiotics showed marked reduction in the total bacterial and *Proteus* abundance by qPCR analyses (Supplementary Figure 4*A* and *B*). Then *P mirabilis* strains W5 (from stool) and W19 (from mucosa), which were isolated from 2 different patients with CD, were introduced to the microbiota-depleted mice 2 days after DSS (1.5%) treatment (Figure 4*A*). Mice gavaged with either *P mirabilis* strain resulted in their colonization of colonic tissues (Figure 4*C*), although colonization was stronger for *P mirabilis* strain W19 (Supplementary Figure 4*B*). To examine the tissue localization of *P mirabilis*, we performed fluorescence in situ hybridization using *P mirabilis* probes on colonic tissues (Figure 4*D*). There was a concordant decrease in body weight for both groups of mice compared with those treated with either *E coli* MG1655 or phosphate-buffered saline (Figure 4*E*). The colon lengths of the *P mirabilis*–inoculated mice (5.68 cm for W5 and 5.9 cm for W19) was shortened compared with those of mice treated with *E coli* MG1655 (6.52 cm) or phosphate-buffered saline (6.95 cm) (Supplementary Figure 4*C* and Figure 4*F*). The spleens of *P mirabilis*–inoculated mice weighed significantly more and were larger than those of *E coli* M1655 or phosphate-buffered saline–treated mice (Figure 4*G*). The DSS-treated colitis mice colonized with either *P mirabilis* strain showed a more intense local and systemic inflammation as assessed by colonic myeloperoxidase activity (Figure 4*H*). Mice treated sequentially with antibiotics and DSS and then challenged with either *P mirabilis* strain also showed significantly greater severity of inflammation on histopathology, but this effect was not observed in mice challenged with nonpathogenic *E coli* strain MG1655 (Figure 4*I*). Ki67-positive signals were also significantly reduced in *P mirabilis*–inoculated mice (Supplementary Figure 4*D*). Collectively, these findings validate that *P mirabilis* can trigger intestinal and systemic inflammation.

Proteus mirabilis *Is Associated With Bacterial Dysbiosis in Mice*

As we found more substantial bacterial dysbiosis and reduced diversity in CD subjects with high *Proteus* than low *Proteus* abundance and control samples, we assessed

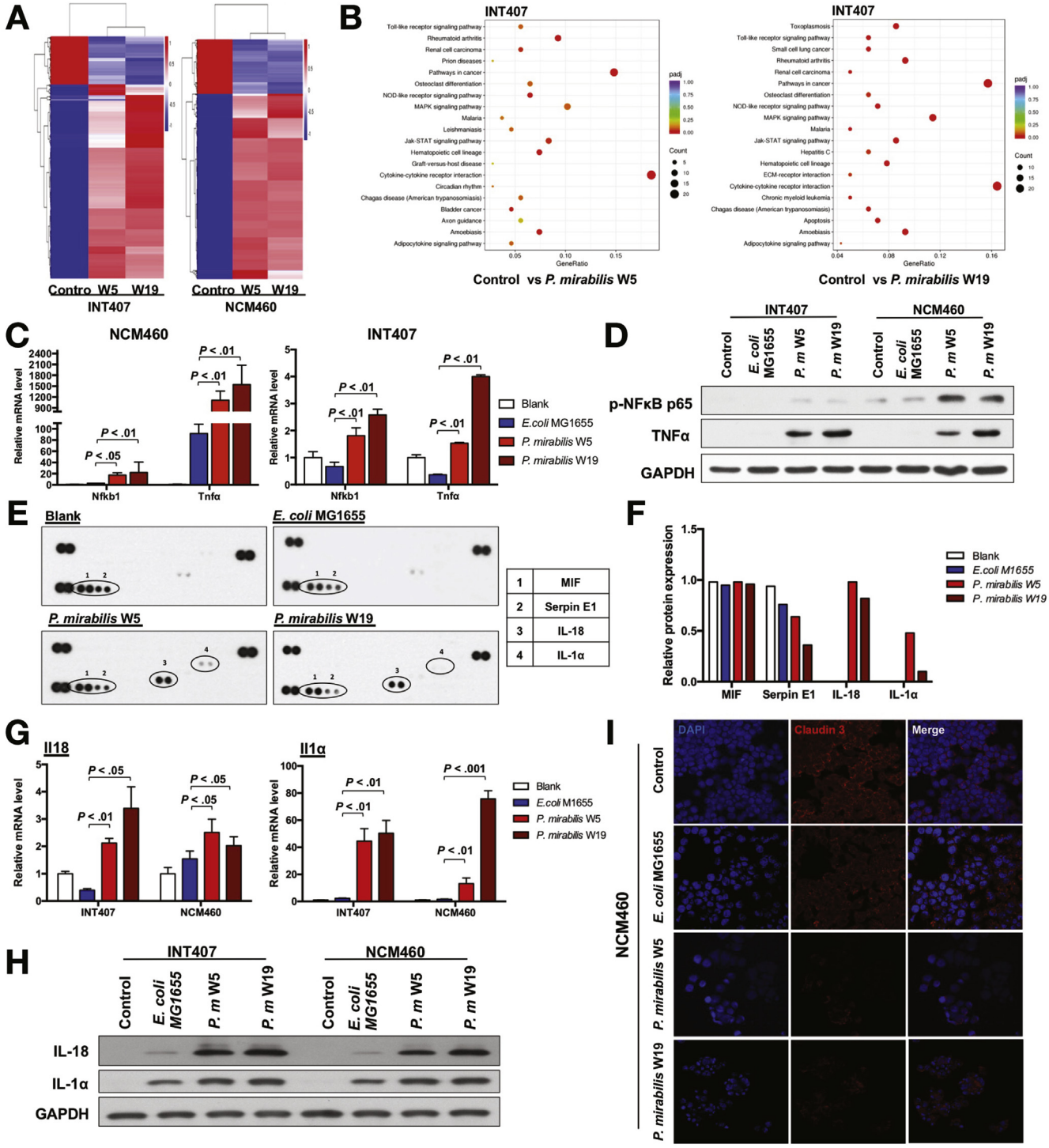

Figure 6. Both *P mirabilis* strain W5 and strain W19 trigger inflammatory gene expression and cytokine secretion from normal epithelial cells. *Heatmap* (*A*) and KEGG pathway analyses (*B*) of the differentially expressed genes from either INT407 or NCM460 cell lines when challenged with either *P mirabilis* strain W5 or strain W19, compared with phosphate-buffered saline controls. Both quantitative reverse transcription PCR (*C*) and Western immunoblot (*D*) analyses verified the expression of pro-inflammatory pathways in both types of cell lines compared with cells challenged with either sterile bacterial culture medium or nonpathogenic *E coli* M1655. Cytokine array membrane profiles (*E*) and cytokine quantification (*F*) from INT407 cells shows IL-18 and IL-1α release is stimulated by *P mirabilis* strains W5 and W19 but not by nonpathogenic *E coli* M1655 or controls. rs, reference spots represent an internal control. The relative amount of IL-18 and IL-1α messenger RNA expression (*G*) and protein levels (*H*) from both INT407 and NCM460 cells are increased by challenge with *P mirabilis* strains W5 and W19. (*I*) Immunofluorescence staining of NCM460 shows Claudin-3 levels (*red*) are reduced from cells challenged with *P mirabilis* strains W5 and W19. The cell nuclei are stained with 4′,6-diamidino-2-phenylindole (*blue*).

whether *P mirabilis* also alters the colonic bacterial communities in the 2 mouse models used here. The 16S ribosomal RNA amplicon profiles showed that the *P mirabilis*–inoculated mice from both models clustered together and the relative abundance of the Phylum *Proteobacteria* is increased, and phylum *Firmicutes* is decreased, compared with the normal and *E coli* MG1655-inoculated mice (Figure 4*J* and *K*). The differentially altered bacterial phyla in mice were consistent with the observation seen in human biopsy samples.

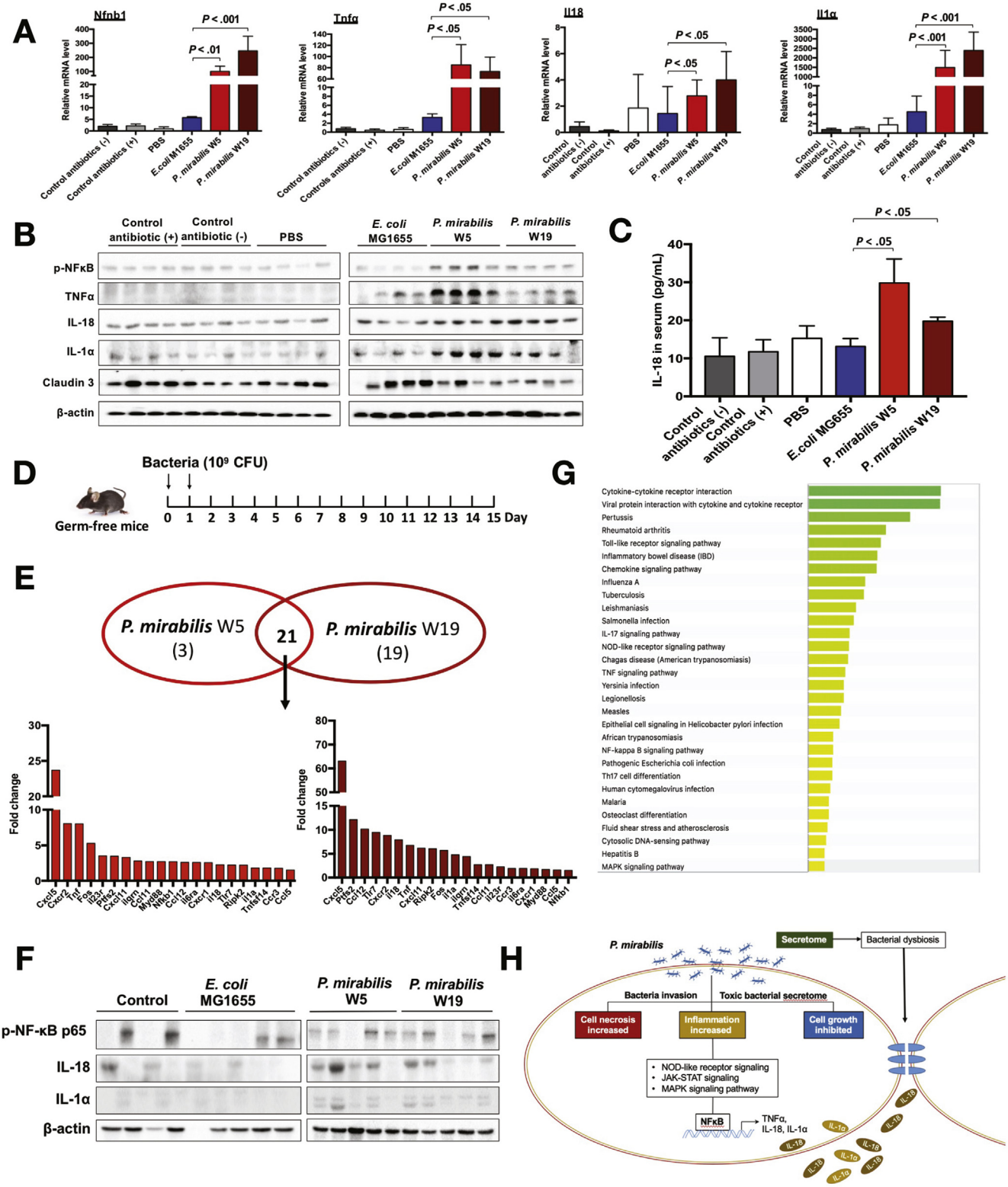

Proteus mirabilis *Strains Are Enteroinvasive and Induce Cell Death In Vitro*

To study the effects of isolated *P mirabilis* strains W5 and W19 on human colonic epithelial cells, we established an in vitro microbe-enterocyte co-culture system. The 2 *P mirabilis* strains, as well as *E coli* strain MG1655 were each cultured with 2 normal epithelial cell lines INT407 and NCM460 and 2 colorectal cancer cell lines $CaCO_2$ and HT29. Microscopic analysis of the cells co-cultured with either *P mirabilis* strain showed they were unhealthy or dead, and cells cultured with medium alone or *E coli* MG1655 remained normal (Figure 5*A*). The morphology of the cells cultured with *P mirabilis* before cell death at 1 hour, 2 hours, and 3 hours showed more unattached and floating cells in cells cultured with *P mirabilis* compared with the control and *E coli* MG1655 groups. Through fluorescence staining, there were increased necrotic cell counts in the *P mirabilis*–challenged cell lines compared with controls (Figure 5*B*). We evaluated whether *P mirabilis* could invade INT407, NCM460, CaCo2, and HT29 cells to cause cell death. Adherent-invasive *E coli* and *P mirabilis* strains W5 and W19 were inoculated into these cell lines. We observed stronger adhesive and invasive ability of the *P mirabilis* strains compared with adherent-invasive *E coli* (Supplementary Figure 5*A*). Further, normal colonic epithelial cell lines inoculated with either *P mirabilis* strain were labeled with the *P mirabilis*–specific fluorescent probe, and confocal microscopy showed abundant bacteria within cell cytoplasm (Figure 5*C*). The positive expression of invasion-related genes further confirmed the invasive ability of *P mirabilis* strains W5 and W19 (Supplementary Figure 5*B*). Under transmission electron microscopy, both *P mirabilis* strains were attached to and invaded all normal colon cell lines but this was not observed with colonic cell lines challenged with *E coli* MG1655 (Figure 5*D*).

Metabolites of Proteus Mirabilis *Strains Induce Cell Death and Inhibit Cell Proliferation*

Cultures of *P mirabilis* strains W5 and W19, as well as *E coli* MG1655, were harvested after overnight growth and the fluid-based "secretome" was produced by filter sterilization. The preparations from both *P mirabilis* strains produced a greater amount of cell apoptosis compared with similar preparations *E coli* MG1655 group (Figure 5*E*) and inhibited both INT407 and NCM460 cell proliferation ($P < .05$) (Figure 5*F*).

Proteus mirabilis *Strains Induce Pro-Inflammatory Pathways and Cytokine Production*

The gene expression profiles from INT407 and NCM460 cells challenged with either *P mirabilis* W5 or W19, or without challenge, was assessed by RNA sequencing and the results are shown in Figure 6*A*, with the enriched signaling pathways modulated in response to the *P mirabilis* strains shown in Figure 6*B* and Supplementary Figure 6. Based on the KEGG annotation's 3 pathways, namely, NOD-like receptor signaling, JAK-STAT signaling, and MAPK signaling pathways were commonly up-regulated both cell lines in response to both *P mirabilis* strains (Figure 6*B*). Moreover, both NF-κB activation and TNFα expression were enhanced in cells cultured with either *P mirabilis* strain, as assessed by Western blot and qPCR (Figure 6*C* and *D*). The cytokine profiles produced from the INT407 and NCM460 cell lines are shown in Figure 6*E*. Both IL-18 and IL-1α secretion were significantly increased in response to challenging these cell lines with *P mirabilis* culture fluids compared with the control groups (Figure 6*F*). We examined intracellular messenger RNA levels of IL-18 and IL-1α in 2 normal cells (INT407, NCM460) and found up-regulated IL-18 and IL-1α mRNA in *P mirabilis*–inoculated cells (Figure 6*G*). Concurrently, intracellular IL-18 protein was also increased in *P mirabilis*–inoculated cells (Figure 6*H*). As IL-18 has been shown to contribute to the breakdown of the mucosal barrier, we further demonstrated the reduced integrity by immunofluorescence assay and decreased protein expression of tight junction marker Claudin-3 in *P mirabilis*–inoculated NCM460 cells (Figure 6*I*).

Proteus mirabilis *Activates NF-κB Signaling and Promotes Secretion of IL-18 in Dextran Sulfate Sodium Mice*

The quantitative reverse transcription PCR analyses of colonic tissues from DSS-treated mice inoculated with either *P mirabilis* strain showed there was a significant up-

Figure 7. Antibiotic-treated and gnotobiotic murine models show both *P mirabilis* strains activate NFκB-directed inflammatory pathways and the secretion of IL-18 and IL-1α to promote inflammation progression in vitro. (*A*) qPCR analysis of NFκB and identified downstream genes in colonic tissues collected from DSS-treated mice (n = 5). (*B*) Western blot and quantitative analysis of the Claudin-3, NFκB, and identified downstream targets. β-actin was used as the loading control. (*C*) Serum IL-18 concentrations were examined in DSS mice by enzyme-linked immunosorbent assay. (*D*) Germ-free mice received doses of either *P mirabilis* strains W5 or W19 for 2 consecutive days at the beginning of the experiment and followed up for 2 weeks. (*E*) The differentially expressed genes in colonic tissues were identified using the mouse inflammatory response and autoimmunity PCR array. A total of 21 genes were up-regulated in response to inoculation with *P mirabilis* strain W5 or *P mirabilis* strain W19 and the fold-changes of these specific genes are shown. (*F*) Protein levels of p-P65, IL-18, and IL-1α were confirmed in colonic tissues from germ-free mice. (*G*) Pathway analysis demonstrates the significant pathways of differentially up-regulated genes in *P mirabilis* group vs control group. (*H*) Proposed mechanistic scheme of *P mirabilis*–mediated intestinal inflammation. *P mirabilis* induces cell necrosis and inhibits cell proliferation via bacterial invasion and their secretion of toxic substances. In addition, *P mirabilis* also enhances the NF-κB–activated immune gene expression and production of TNFα, IL-18, and IL-1α. The elevated levels of IL-18 and IL-1α can result in the disturbance of cell tight junctions, further leading to the translocation of other members of the gut microbiota. Taken together *P mirabilis* induces and maintains Crohn's disease inflammation in intestinal epithelial cells.

regulation of TNFα, IL-18, and IL-1α, as well as a down-regulation of Claudin-3 (Figure 7*A*). In addition, protein expression of p-NF-κB p65, TNFα, IL-18, and IL-1α were all up-regulated, and Claudin-3 was decreased in the colonic tissue of *P mirabilis*–treated DSS mice (Figure 7*B*). Enhanced level of IL-18 secretion was also observed in serum of the mice infected with *P mirabilis* (Figure 7*C*).

Germ-Free Mice Gavaged With Proteus mirabilis *Show Increased Expression of Pro-Inflammatory Genes*

We used a germ-free mouse model to further confirm the pathogenicity of *P mirabilis* (Figure 7*D*). We studied the gene expression profile of colonic cells 2 weeks after gavaged with *P mirabilis* W5, W19, and control *E coli* MG1655, respectively, using PCR array (covering 84 key genes involved in the inflammatory response). We found 24 genes and 40 genes in mice gavaged with *P mirabilis* W5 and W19 were up-regulated compared with the *E coli* MG1655 infected group. Among them, 21 up-regulated proinflammatory genes were shared by these 2 groups of mice (Figure 7*E*, Supplementary Table 7). Genes involved in the NF-κB signaling, including NF-κB1, TNF, and TNFsf14 were up-regulated. Neutrophil chemotaxis associated gene Cxcl5 and its receptor Cxcr2 which usually enhanced in IBD patients were also up-regulated. The enhanced protein expression of NF-κB, IL-18 and IL-1α were confirmed by Western blot (Figure 7*F*). KEGG pathway analysis revealed the enriched pathways induced by *P mirabilis* include inflammatory bowel disease, Toll-like receptor, NOD-like receptor, MAPK, and NF-κB signaling (Figure 7*G*). These data support that *P mirabilis* is capable of inducing pro-inflammatory genes and activating inflammation-related pathways in germ-free mice, confirming its potential functional significance as a pathobiont bacteria in CD development.

Discussion

Proteus spp and related bacteria are widely considered to be microbes of low abundance within the human gastrointestinal tract. Given that the bioinformatic workflows used with most stool microbiome data sets exclude taxa found at <0.1% relative abundance, this might account for the genus *Proteus* not being detected consistently and reported in previous studies. Nonetheless their virulence factors and physiologic attributes (eg, motility and swarming) have been well characterized in urinary tract infections, and these features bear clinical relevance in terms of their potential role as gastrointestinal pathogens.[20] In this study, we found that although reads assigned to the genus *Proteus* were present from the stool samples of both healthy subjects and patients with CD, reads assigned to this genus were more prevalent and present in greater abundance in patients with CD, and particularly from mucosal tissue samples. Such findings imply that *Proteus* spp might act as pathobionts rather than an obligate pathogen, and under the right enteric environment could expand and exhibit virulence characteristics, akin to another well-described pathobiont, *Helicobacter pylori*. We were able to stratify our CD cohort into a high *Proteus* or low *Proteus* group, and found that the clinical activity of CD was more severe for the former group. Crohn's disease activity index and *Proteus* abundance do not establish causality. However, they likely add support to the relationship between *Proteus* spp and inflammation. The high *Proteus* group also had decreased relative abundance of *Faecalibacterium* spp and greater abundance of *Fusobacterium* spp. These data, together with earlier work showing low abundance of *Faecalibacterium* spp and presence of *Proteus* spp (odds ratio, 13) as a risk factor of disease recurrence,[8] suggest a key role for *Proteus* spp in CD pathophysiology.

Proteus-associated intestinal dysbiosis was associated with reduced bacterial diversity, particularly in those patients in the high *Proteus* group. As expected, the relative abundance of *Proteobacteria* was increased and *Firmicutes* reduced in these patients, but members of the *Bacteroidetes* and *Fusobacterium* spp were also more likely to form strong co-occurring relationships. These interrelationships reflect how the mucosa-associated bacteria can promote gut inflammation and that high *Proteus* patients with CD face a greater risk of disease recurrence.

Importantly, we found that all of the isolates recovered from stool and mucosa of CD belonged to *P mirabilis*. Interestingly though, a combination of 16S ribosomal RNA gene and whole-genome–based phylogenetic analyses of these strains and comparison with other publicly available *P mirabilis* genomes revealed a strain-based variation existed between our isolates of stool or tissue origin. Based on the average nucleotide identity scores *P mirabilis* strains W1–W12, which are all recovered from stool samples, most likely represent the same clonal lineage. To our knowledge however, *P mirabilis* strains W19–W24 are the first to be recovered from colonic tissue biopsies, and these strains are clearly separable from the stool isolates. This veracity of these differences is augmented by inclusion of genome data from 33 other *P mirabilis* strains recovered from both urine and stool.

For these reasons, the subsequent series of in vivo and in vitro studies with *P mirabilis* strains W5 and W19 were done to evaluate whether there might be a differential effect from these strains on host/cellular response. Based on the collective in vitro and in vivo studies, both *P mirabilis* strains were capable of inducing cell necrosis and inhibiting cell growth via bacteria invasion and/or the release of toxic substances. Both of the *P mirabilis* strains examined here also increase the expression of 3 key pro-inflammatory pathways and stimulate the production of pro-inflammatory cytokines. The pathogenic role of both strains was also confirmed in germ-free animals mono-associated with either of these *P mirabilis* strains.

The inter-strain comparisons showed that although *P mirabilis* strains W5 and W19 both share extensive genetic synteny with *P mirabilis* HI4320, there were some key differences with respect to fimbrial gene density. *P mirabilis* strain W19, as well as the majority of our isolates from biopsy tissue, possess a greater number of genes involved

with fimbrial structure-function than our isolates from stool samples. More specifically, the 2 strains appear to be differentiated by the presence of genes putatively encoding for K- and II-type fimbriae and chaperone/usher functions. However, the majority of singleton genes identified for both strains W5 and W19 remain obscure as hypothetical proteins. As such, although the greater density of fimbriae-related genes in the *P mirabilis* strains isolated from biopsy tissue might be distinctive with respect to their adhesion properties, the exact mechanisms giving rise to the strain differences and cellular response remain unclear.

Several microbes have been reported as direct or indirect triggers for CD progression. The *Enterococci* and *Clostridium perfringens* can generate a complement of extracellular toxins and hydrolytic enzymes (>20), which induce various histotoxic infections in colon.[15] *Bacteroides fragilis*, through secretion of its proinflammatory toxin, are capable of initiating an inflammatory mucosal immune response that contributes to initiation and/or exacerbation of inflammatory bowel disease[21] adherent-invasive *E coli* virulence properties are linked to their survival and replication within macrophages.[22]

Elevated levels of urease activity have recently been identified as one of the key functional changes associated with the microbial dysbiosis in association with CD.[9] In that context, *Proteus* spp and other members of the recently created *Morganellaceae* (fam. nov.), such as *Morganella* and *Providencia* spp, are widely recognized for their production of urease activity.[23]

The RNA sequencing results showed that both the *P mirabilis* strains enhanced the expression of 3 main pro-inflammatory pathways, including NOD-like receptor signaling, Jak-STAT signaling, and MAPK signaling pathways. Both *P mirabilis* whole cells, and its virulent byproducts may bind to TLRs and induce NF-κB–dependent gene expression via MAPK pathway. The activation of NF-κB and MAPK is quick and helps to produce pro-inflammatory cytokines, such as TNFα, IL-18, and IL-1α. The NOD-like receptor family plays an important role in intracellular ligand recognition, followed by activation of NF-κB and MAPK cytokine production. The produced cytokines may trigger innate or adaptive immune responses by binding to specific receptors on macrophage and other immune cell surfaces and resulting in host defense, cell death, and chronic inflammatory infiltration. These regulated pro-inflammatory genes and pathways were observed in the *P mirabilis* inoculated germ-free mouse model. Unlike manipulation of the microbiota through antibiotics, the germ-free mouse is generally considered to be the reference standard for studies of the microbiota.[24] It can contribute to determine how specific microbiomes protect from or contribute to disease progression. Putting these characteristics together, *Proteus* spp might be involved in the development of CD through specific mechanisms and signaling pathways.

In conclusion, we have found that *P mirabilis* is more prevalent in the mucosa and feces of patients with CD. Functional studies demonstrated potent pathologic features, including colonic epithelial cell invasion. Animal models demonstrated that colonization of *P mirabilis* promotes colonic inflammation by inducing pro-inflammatory pathways and cytokines. These findings demonstrate a novel mechanism of *P mirabilis*–induced inflammation in the development of CD. As such *P mirabilis,* and most likely related bacteria such as *Morganella* and *Providencia* spp warrant greater consideration as a key microbial trigger in the pathogenesis of CD and as a diagnostic and therapeutic target to improve patient recovery and remission.

Supplementary Material

Note: To access the supplementary material accompanying this article, visit the online version of *Gastroenterology* at www.gastrojournal.org, and at https://doi.org/10.1053/j.gastro.2020.09.036.

References

1. Gevers D, Kugathasan S, Denson LA, et al. The treatment-naive microbiome in new-onset Crohn's disease. Cell Host Microbe 2014;15:382–392.
2. Farrell RJ, LaMont JT. Microbial factors in inflammatory bowel disease. Gastroenterol Clin North Am 2002; 31:41–62.
3. Sartor RB. Intestinal microflora in human and experimental inflammatory bowel disease. Curr Opin Gastroenterol 2001;17:324–330.
4. Manichanh C, Rigottier-Gois L, Bonnaud E, et al. Reduced diversity of faecal microbiota in Crohn's disease revealed by a metagenomic approach. Gut 2006; 55:205–211.
5. Cotter PD. Small intestine and microbiota. Curr Opin Gastroenterol 2011;27:99–105.
6. Kamada N, Chen GY, Inohara N, et al. Control of pathogens and pathobionts by the gut microbiota. Nat Immunol 2013;14:685–690.
7. Raes J. Microbiome-based companion diagnostics: no longer science fiction? Gut 2016;65:896–897.
8. Wright EK, Kamm MA, Wagner J, et al. microbial factors associated with postoperative Crohn's disease recurrence. J Crohns Colitis 2017;11:191–203.
9. Ni J, Shen TD, Chen EZ, et al. A role for bacterial urease in gut dysbiosis and Crohn's disease. Sci Transl Med 2017;9:eaah6888.
10. **Adeolu M, Alnajar S**, Naushad S, et al. Genome-based phylogeny and taxonomy of the 'Enterobacteriales': proposal for Enterobacterales ord. nov. divided into the families Enterobacteriaceae, Erwiniaceae fam. nov., Pectobacteriaceae fam. nov., Yersiniaceae fam. nov., Hafniaceae fam. nov., Morganellaceae fam. nov., and Budviciaceae fam. nov. Int J Syst Evol Microbiol 2016; 66:5575–5599.
11. Chew R, Thomas S, Mantha ML, et al. Large urate cystolith associated with *Proteus* urinary tract infection. Kidney Int 2012;81:802.
12. Ahmed M. Acute cholangitis—an update. World J Gastrointest Pathophysiol 2018;9:1–7.

13. Singh R, Kumar N, Sundriyal D, et al. Mixed pyogenic and tuberculous liver abscess: clinical suspicion is what matters. BMJ Case Rep 2013;2013.
14. Sogaard KK, Thomsen RW, Schonheyder HC, et al. Positive predictive values of the International Classification of Diseases, 10th revision diagnoses of Gram-negative septicemia/sepsis and urosepsis for presence of Gram-negative bacteremia. Clin Epidemiol 2015; 7:195–199.
15. Hamilton AL, Kamm MA, Ng SC, et al. *Proteus* spp as putative gastrointestinal pathogens. Clin Microbiol Rev 2018;31:bcr2013008768.
16. Chen CY, Chen YH, Lu PL, et al. *Proteus* mirabilis urinary tract infection and bacteremia: risk factors, clinical presentation, and outcomes. J Microbiol Immunol Infect 2012;45:228–236.
17. Roach DJ, Burton JN, Lee C, et al. A year of infection in the intensive care unit: prospective whole genome sequencing of bacterial clinical isolates reveals cryptic transmissions and novel microbiota. PLoS Genet 2015; 11:e1005413.
18. Shi X, Zhu Y, Li Y, et al. Genome sequence of *Proteus* mirabilis clinical isolate C05028. Genome Announc 2014; 2(2):e00167-14.
19. Johnning A, Karami N, Tang Hallback E, et al. The resistomes of six carbapenem-resistant pathogens—a critical genotype-phenotype analysis. Microb Genom 2018;4(11):e000233.
20. McClane BA, Uzal FA, Miyakawa MEF, et al. The enterotoxic Clostridia. In: Dworkin M, Falkow S, Rosenberg S, et al, eds. *Prokaryotes: A Handbook on the Biology of Bacteria*. 3rd ed.Volume 4. Basel, Switzerland: Springer, 2006:698–752.
21. Robizadeh S, Rhee KJ, Wu SG, et al. Enterotoxigenic *Bacteroides fragilis*: a potential instigator of colitis. Inflamm Bowel Dis 2007;13:1475–1483.
22. Nguyen HTT, Lapaquette P, Bringer MA, et al. Autophagy and Crohn's disease. J Innate Immun 2013;5:434–443.
23. O'Hara CM, Brenner FW, Miller JM. Classification, identification, and clinical significance of *Proteus, Providencia*, and *Morganella*. Clin Microbiol Rev 2000;13:534–546.
24. Kennedy EA, King KY, Baldridge MT. Mouse microbiota models: comparing germ-free mice and antibiotics treatment as tools for modifying gut bacteria. Front Physiol 2018;9:1534.

Author names in bold designate shared co-first authorship.

Received June 3, 2020. Accepted September 23, 2020.

Correspondence
Address correspondence to: Siew C. Ng, PhD, Department of Medicine and Therapeutics, The Chinese University of Hong Kong, 9/F, Lui Che Woo Clinical Sciences Building, Prince of Wales Hospital, Shatin, Hong Kong, China. e-mail: siewchienng@cuhk.edu.hk; Mark Morrison, PhD, University of Queensland Diamantina Institute, Translational Research Institute, Level 6E, 37 Kent Street, Woolloongabba, QLD. 4102, Australia. e-mail: m.morrison1@uq.edu.au; Jun Yu, PhD, Department of Medicine and Therapeutics, The Chinese University of Hong Kong, Rm707, Li Ka Shing Medical Sciences Building, Prince of Wales Hospital, Shatin, Hong Kong, China. e-mail: junyu@cuhk.edu.hk; or Michael Kamm, PhD, Department of Medicine, The University of Melbourne, Victoria Parade Fitzroy 3065, Melbourne, Australia. e-mail: mkamm@unimelb.edu.au.

CRediT Authorship Contributions
Jingwan Zhang, PhD (Conceptualization: Lead; Data curation: Lead; Investigation: Lead; Methodology: Lead; Writing – original draft: Lead).
Emily C. Hoedt, PhD (Formal analysis: Lead; Writing – original draft: Equal).
Qin Liu, PhD (Data curation: Supporting; Methodology: Equal).
Erwin Berendsen, PhD (Formal analysis: Equal; Software: Equal).
Jing Jie Teh, Postgraduate (Formal analysis: Supporting; Software: Supporting).
Amy Hamilton, PhD (Funding acquisition: Supporting; Resources: Supporting).
Amy Wilson O' Brien, PhD (Funding acquisition: Supporting; Project administration: Supporting).
Jessica Ching, Postgraduate (Funding acquisition: Equal; Project administration: Equal; Resources: Equal).
Hong Wei, PhD (Investigation: Supporting; Resources: Equal).
Keli Yang, Postgraduate (Formal analysis: Lead; Software: Equal).
Zhilu Xu, PhD (Methodology: Supporting; Validation: Supporting).
Sunny H Wong, PhD (Conceptualization: Supporting; Writing – review & editing: Supporting).
Joyce W. Y. Mak, PhD (Resources: Equal).
Joseph J. Y. Sung, PhD (Funding acquisition: Supporting; Project administration: Equal).
Mark Morrison, PhD (Funding acquisition: Equal; Project administration: Equal; Writing – review & editing: Equal).
Jun Yu, PhD (Conceptualization: Supporting; Writing – review & editing: Equal).
Michael A Kamm, PhD (Funding acquisition: Lead; Project administration: Lead; Writing – review & editing: Equal). Siew C Ng, PhD (Funding acquisition: Lead; Supervision: Lead; Writing – review & editing: Equal).

Conflicts of interest
The authors disclose no conflicts.

Funding
Supported by The Leona M. and Harry B. Helmsley Charitable Trust and Croucher Senior Medical Research Fellowship. The Translational Research Institute is funded by a grant from the Australian Federal Government.

DNA Extraction and *Proteus spp* Quantification

For optimal isolation of bacterial DNA, mucosal biopsies were disrupted by bead-beating upon digestion in lysozyme (Sigma Aldrich, Northbrook, IL) before extraction and purification by QIAamp DNA Mini Kit. Stool DNA was extracted by Mobio PowerSoil DNA Isolation kit (Qiagen, Hilden, Germany). DNA was quantified using NanoDrop2000 spectrophotometer (ThermoFisher Scientific, Waltham, MA).

Real-Time Polymerase Chain Reaction

Quantitative PCR was performed with 1 μL of DNA (0.5 ng) in each 20 μL of Universal SYBR Green Master (Roche, Risch-Rotkreuz, Switzerland) reaction. The reaction was performed in triplicate and analyzed on QuantStudio 7 Flex System (ThermoFisher Scientific). The following primer sets were used: primers for *Proteus* spp detection, UreR, forward (5′→3′) GGT GAG ATT TGT ATT AAT GG; reverse (5′→3′) ATA ATC TGG AAG ATG ACG AG and UreC, forward (5′→3′) CCG GAA CAG AAG TTG TCG CTG GA; reverse (5′→3′) GGG CTC TCC TAC CGA CTT GAT C. Primer for total bacteria detection, 16s, forward (5′→3′) CGG CAA CGA GCG CAA CCC; reverse (5′→3′) CCA TTG TAG CAC GTG TGT AGC C.

16S Sequencing and Analysis

16S ribosomal RNA gene amplicon sequencing was performed on DNA extracted from 63 biopsy samples (25 normal and 38 CD). The V3-V4 hypervariable region of 16S ribosomal RNA gene was amplified by forward primer 341F-CCTAYGGGRBGCASCAG and reverse primer 806R-GGACTACNNGGGTATCTAAT. Illumina HiSeq 2500 platform (Illumina, San Diego, CA) was used to generate PE 250 bp raw reads by Novogene (Beijing, China). The sequencing raw reads were demultiplexed and adapter trimming was done using QIIME, version 1.7.0 (qiime2.org/). Further reads were imported to QIIME2, version 2019.1, for quality control and operational taxonomic unit table generated. The DADA2 plugin in QIIME2 was used to generate exact sequence variants, which were classified by naïve Bayes classifier from Greengenes database (version 13.8, trimmed to V3–V4 primer region and trained on 99% operational taxonomic units).

The majority of statistical analyses and visualizations were done in Rstudio and R, version 3.51 (www.r-project.org). The bacterial operational taxonomic unit table was imported into R by Phyloseq package and process by Tidyverse packages. Richness and diversity were performed using the estimated richness function of the Phyloseq and Vegan package. The operational taxonomic unit read counts were normalized by cumulative sum scaling method using MetagenomeSeq R/Bioconductor package before calculating Bray Curtis dissimilarity distances. Visualization of figures were done by ggplot2, ggpubr, and pheatmap R package. Linear discriminant analysis effect size analysis was performed to define biomarkers between groups.

Co-Occurrence and Co-Exclusion Analysis

Co-occurrence and co-exclusion relationships between groups were estimated using SparCC algorithm. For the correlation pairs, only P values $<.05$ were considered significant. For visualization, correlations with absolute coefficients <0.3 were masked to show all signals that were exclusively significant.

Bacterial Culture

Isolated *Proteus* spp were maintained in lysogeny broth or MacConkey broth (#70144-500G; Sigma-Aldrich, West Palm Beach, FL) under aerobic conditions with shaking overnight. Where appropriate, *E coli* strain MG1655 was used as a control for comparative assays with the *Proteus* isolates and was also cultured using lysogeny broth and aerobic conditions.

Genomic and Plasmid DNA Extraction and Sequencing

The genomic DNA from 24 isolates of candidate *Proteus* spp was extracted using the QIAamp DNA Mini Kit according to the manufacturer's instructions, and then used for genome sequencing via BGI (https://www.bgi.com/global/) with the Illumina NextSeq 4000 platform (2 × 150 bp). The sequence data were quality checked, filtered, and then the forward and reverse reads were assembled de novo using Unicycler Galaxy, version 0.4.6.0. (The University of Melbourne, Victoria, Australia) The quality of the genome assemblies and contamination scores were assessed using CheckM (The University of Queensland, Queensland, Australia). This Whole Genome Shotgun projects have been deposited at DDBJ/ENA/GenBank under accessions SDEQ00000000, SDER00000000, SDES00000000, SDES00000000, SDET00000000, SDEU00000000, SDEV00000000, SDEW00000000, SDEX00000000, SDEY00000000, SDEZ00000000, SDFA00000000, SDFB00000000, SDFC00000000, SDFD00000000, SDFE00000000, SDFF00000000, SDFG00000000, SDFH00000000, SDFI00000000, SDFJ00000000, SDFK00000000, SDFL00000000, SDFM00000000, SDFN00000000. The version described in this article is version SDEQ01000000, SDER01000000, SDES01000000, SDES01000000, SDET01000000, SDEU01000000, SDEV01000000, SDEW01000000, SDEX01000000, SDEY01000000, SDEZ01000000, SDFA01000000, SDFB01000000, SDFC01000000, SDFD01000000, SDFE01000000, SDFF01000000, SDFG01000000, SDFH01000000, SDFI01000000, SDFJ01000000, SDFK01000000, SDFL01000000, SDFM01000000, SDFN01000000.

P mirabilis *Phylogeny and Comparative Genomic Analyses*

The data produced for the 24 clinical isolates outlined above were augmented with an additional 33 *P mirabilis* genomes recovered from the National Center for Biotechnology Information database representing both gut and

urinary tract isolates. The phylogeny was first compared by 16S ribosomal RNA gene sequence alignments using SILVA. The phylogenetic tree was constructed from 1000 bootstrap replications with Kimura 2-parameter modeling using MEGA 7. The basic genome metrics for the clinical isolates and previously deposited genomes are summarized in Supplementary Table 2. The genome assemblies for all 24 clinical isolates were annotated using Prokka (Monash University, Australia), RAST version 2.0 (PATRIC), and National Center for Biotechnology Information. For genomic comparisons, the isolates and publicly available genomes were then uploaded to the software platform EDGAR[21] to determine a core, shared and accessory genome. The average nucleotide identity scores between the orthologs present in a "core genome" from all 57 *P mirabilis* genomes were also calculated using EDGAR, and a matrix of average nucleotide identity scores generated using RStudio. For the pan/core genome development plots, the Pangenome Analysis Pipeline standalone tool[1] was employed through BioLinux (http://environmentalomics.org/bio-linux/). The annotation (.ptt), nucleotide sequences (.nuc), and protein sequences (.pep) files were generated with Prokka and formatted with Biolinux. The Pangenome Analysis Pipeline analysis pipeline provided gene clusters assigned to either the core or pan-genome, and visualized using the software package PanGP. The core genome faa (amino acid) output file generated by EDGAR was submitted to KEGG KOALA (https://www.kegg.jp/blastkoala/) for comprehensive assessment of functional categories conserved across all genomes. Finally, the whole-genome–based phylogeny of the *P mirabilis* strains selected for these studies was determined using the Genome Trees Database, which uses the concatenation of 120 universal marker genes to perform the analysis.[2]

Two *P mirabilis* clinical isolates were chosen for the in vitro and in vivo studies outlined below: 1 from the stool sample (W5) of patient BX537, and another from the biopsy sample (W19) from patient BX1226. These *P mirabilis* isolates are hereafter referred to as strain W5 and strain W19 and were first compared using Mauve (the Darling lab) to assess the extent of genome synteny (and differences) between these 2 strains, and with the *P mirabilis* HI4320 genome used as the reference. Virulence maps for strains W5 and W19 were generated by first identifying RAST-based "Virulence, Disease and Defence" annotations and then mapping these genes to their respective genomes using GView (https://server.gview.ca/). IslandViewer 4 was also used to further identify potential pathogenicity islands, but returned no hits of significance. Shared and singleton genes for each genome were quantified using EDGAR and the faa (amino acid) output file for singleton genes generated by EDGAR submitted to KEGG KOALA (https://www.kegg.jp/blastkoala/) for functional assignments.

Fluorescence in Situ Hybridization

A *P mirabilis*-specific probe (5′-GCCCCTGCTTTGGTC) was labeled with Spectrum-Green (Alexa Fluor-488; ThermoFisher Scientific) and fluorescence in situ hybridization was performed. Briefly, frozen colon tissue was fixed in Carnoy's solution for 4 hours and embedded in paraffin; 5-μm-thick sections were hybridized in the hybridization buffer (0.9M NaCl, 20 mM Tris/HCl, pH 7.3, 0.01% sodium dodecyl sulfate). Stringency was used with the formamide concentration from 0% to 30% (v/v). Prewarmed hybridization buffer (20 mL) was mixed with approximately 5 pmol of the oligonucleotide probe and carefully applied to the tissue sections. After incubation for 5 hours in a dark humid chamber at 37°C, each of the slides were rinsed with sterile double-distilled water, air-dried in the dark, and mounted with ProLong Gold Antifade Mountant with 4′,6-diamidino-2-phenylindole (ThermoFisher Scientific).

Cell Culture

The intestinal epithelial cell line INT407 was provided by a laboratory in France (M2iSH Laboratory, Clermont-Ferrand, France) and the immortalized normal colonic epithelial cell line NCM460 was obtained from In Cell (San Antonio, TX). Colon cancer cell lines HT-29 and Caco-2 were obtained from the American Type Culture Collection (Manassas, VA). All mammalian cells were cultured in Dulbecco's modified Eagle medium (Gibco BRL, Grand Island, New York) supplemented with 10% fetal bovine serum and 1% penicillin/streptomycin. For a single experiment, each epithelial cell line was exposed to either *Proteus* sp W5 or W16, or to *E. coli* MG1655, at a multiplicity of infection of 100 for 4 hours.

Cell Apoptosis Assay

INT407, NCM460, CaCo2, and HT29 cells (2.5×10^4 cells/well) were grown in 24-well plates. After removing the medium, the cells were washed 3 times using phosphate-buffered saline. Apoptosis and necrosis were detected using an Apoptosis Detection Kit (ab176749; Abcam, Cambridge, UK). Fluorescence of cells was examined using a Leica DMi8 microscope (Leica Microsystems, Wetzlar, Germany). Fluorescence was measured and quantified.

Cell Attachment and Invasion Assays

The epithelial cells were grown to confluence in 24-well plates at 1×10^5/well followed with inoculation with suspensions of *Proteus* spp at a multiplicity of infection of 100:1 in epithelial cell media. The epithelial cell monolayers were challenged with strains of *Proteus* spp for 3 hours and incubated in 5% CO_2 at 37°C. Nonadherent bacteria were then removed by washing. Following 1 hour incubation in either epithelial cell media containing 10% phosphate-buffered saline (for enumeration of attached bacteria) or epithelial cell media containing 10% phosphate-buffered saline with 100 μg/mL gentamycin (Sigma) (for enumeration of intracellular invaded bacteria), the monolayers were washed and the epithelial cells were lysed with 1X Triton (Sigma) to release the intracellular bacteria. The number of cells with associated bacteria and intracellular bacteria was enumerated by viable count. Attachment was determined as the proportion of the inoculum that had attached to epithelial cells, and invasion as the proportion of the attached bacteria that had invaded the epithelial cells.

Tissue Collection

The weight of the mice was measured and stool samples were collected daily. Mice were anesthetized with chloroform and sacrificed. The whole colon of the mice was flushed with phosphate-buffered saline and divided into 3 sections (proximal, middle, and distal). The distal part was fixed in 10% buffered formalin and Carnoy's solution, processed, and embedded in paraffin for histologic analyses. The remaining 2 colonic sections were snap-frozen for subsequent molecular analyses. All animal studies were performed in accordance with guidelines approved by the Animal Experimentation Ethics Committee of The Chinese University of Hong Kong and the Third Military Medical University in Chongqing, China.

Histopathology

Colonic specimens were formalin-fixed and paraffin-embedded for histologic examination. Sections of 5 μm were stained with H&E for histologic diagnosis. H&E-stained slides were examined under a light microscope (Olympus BX51; Olympus, Tokyo, Japan) in a double-blind manner by 2 histopathologists who were unaware of the treatment allocation of the mice.

Cell Viability Assay

For cell viability assay, 1×10^4 colon cells were grown in a 24-well plate and co-cultured with Dulbecco's modified Eagle medium supplemented with 20% bacterial culture medium at 37°C condition. MTT cell proliferation array was performed every day for 5 consecutive days.

Western Blot Analysis

Total protein was isolated from cell pellets and separated by sodium dodecyl sulfate polyacrylamide gel electrophoresis. The proteins in sodium dodecyl sulfate polyacrylamide gel electrophoresis were transferred onto polyvinylidene difluoride membranes (BioRad, Hercules, CA). The membranes were incubated with primary and secondary antibodies respectively (IL-18: M156-3; Santa Cruz Biotechnology, Santa Cruz, CA). Band intensities were determined by ImageJ software (National Institutes of Health, Bethesda, MD). The mean value of band intensities from 3 independent experiments was used. The band intensity ratio of a candidate protein to glyceraldehyde 3-phosphate dehydrogenase was calculated.

Human Cytokine Array

Two normal epithelial cell lines INT407 and NCM460 were seeded at 1×10^6 cells/well in 6-well plates and challenged with *P mirabilis* for 3 hours. Control and conditioned medium were collected, filtered through a 0.22-μm filter, and processed with the Proteome Profiler Kit (ARY005B; R&D Systems, Minneapolis, MN) following manufacturer's instructions. Images were quantified using ImageJ software.

References

1. Zhao Y, Wu J, Yang J, et al. PGAP: pan-genomes analysis pipeline. Bioinformatics 2012;28:416–418.
2. Parks DH, Rinke C, Chuvochina M, et al. Recovery of nearly 8,000 metagenome-assembled genomes substantially expands the tree of life. Nat Microbiol 2017; 2:1533–1542.

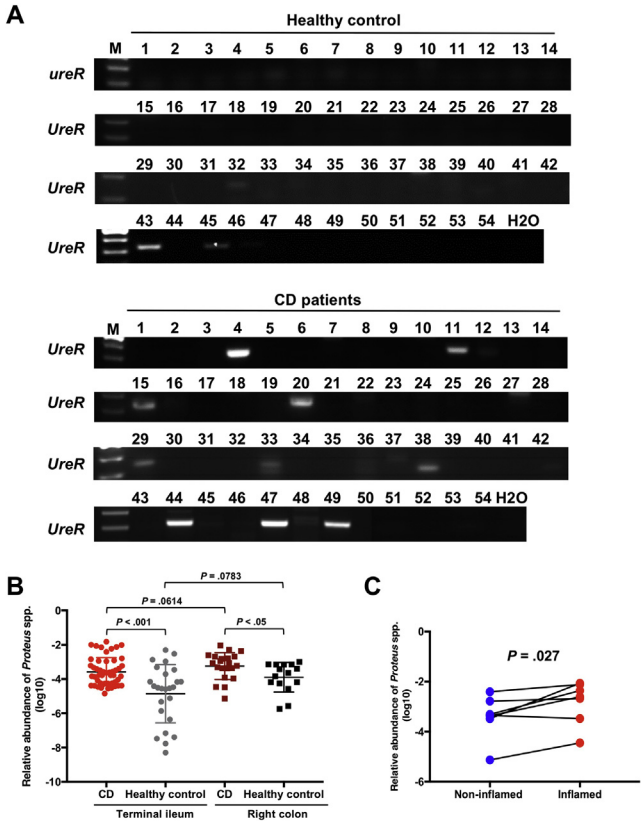

Supplementary Figure 1. (*A*) Presence of *Proteus* spp in total 108 stool samples collected from 54 healthy controls and 54 CD patients. (*B*) Abundance of *Proteus* in CD and healthy controls collected from terminal ileum and right colon. (*C*) Abundance of *Proteus* was higher in inflamed tissue compared with paired nonflamed tissue, which collected from 7 CD patients.

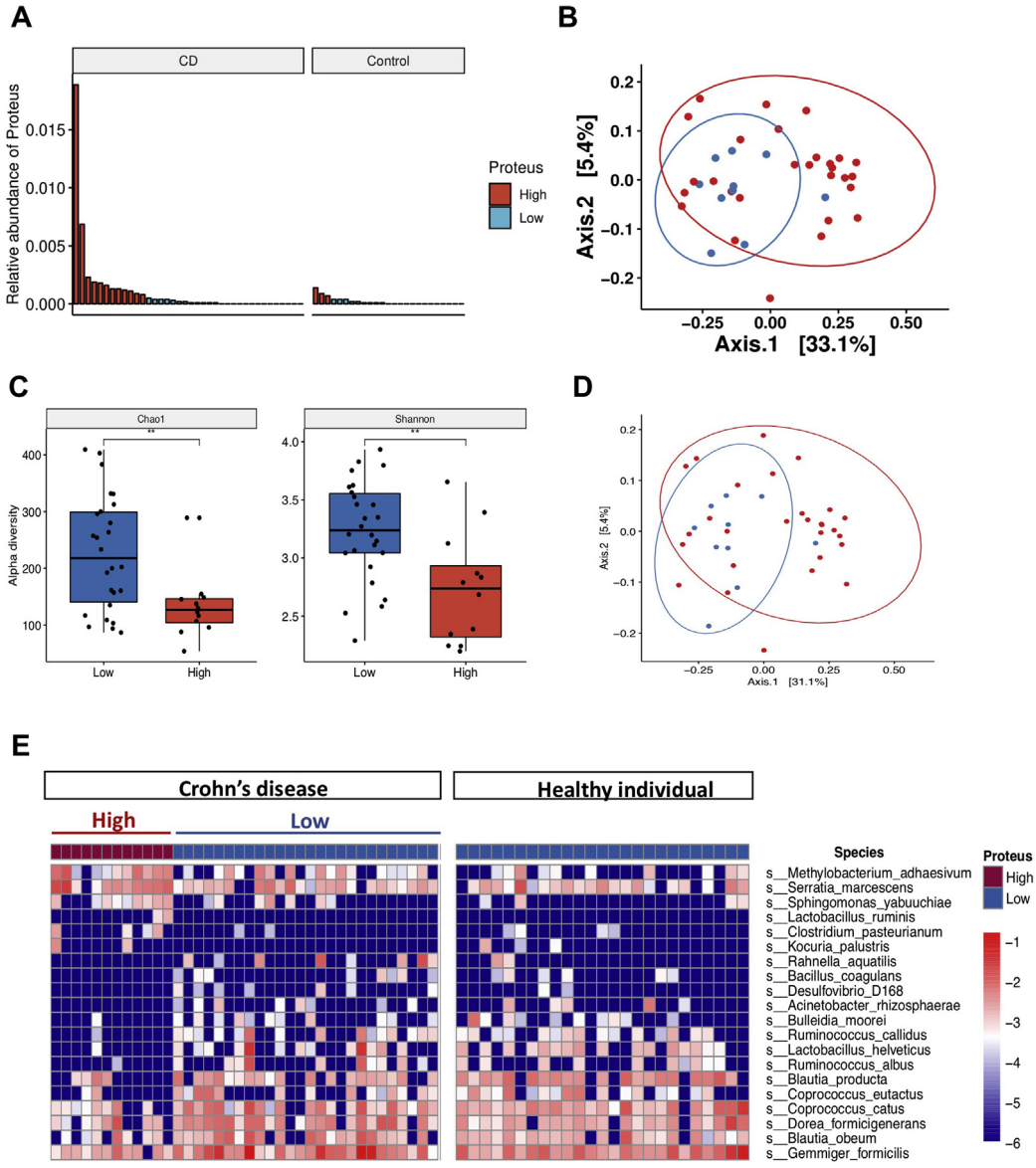

Supplementary Figure 2. (*A*) The abundance of *Proteus* in mucosal samples from 16S ribosomal RNA sequence data. (*B*) Principal coordinates analysis (PCoA) plot of high and low *Proteus* in mucosal samples at genus level. (*C*) Chao1 and Shannon diversity scores are reduced for mucosa-associated microbial communities containing high levels of *Proteus* spp at species level. (*D*) PCoA plot of high and low *Proteus* in mucosal samples at species level. (*E*) The species-level *heatmaps* shows the bacterial profiles from the high and low *Proteus* spp.

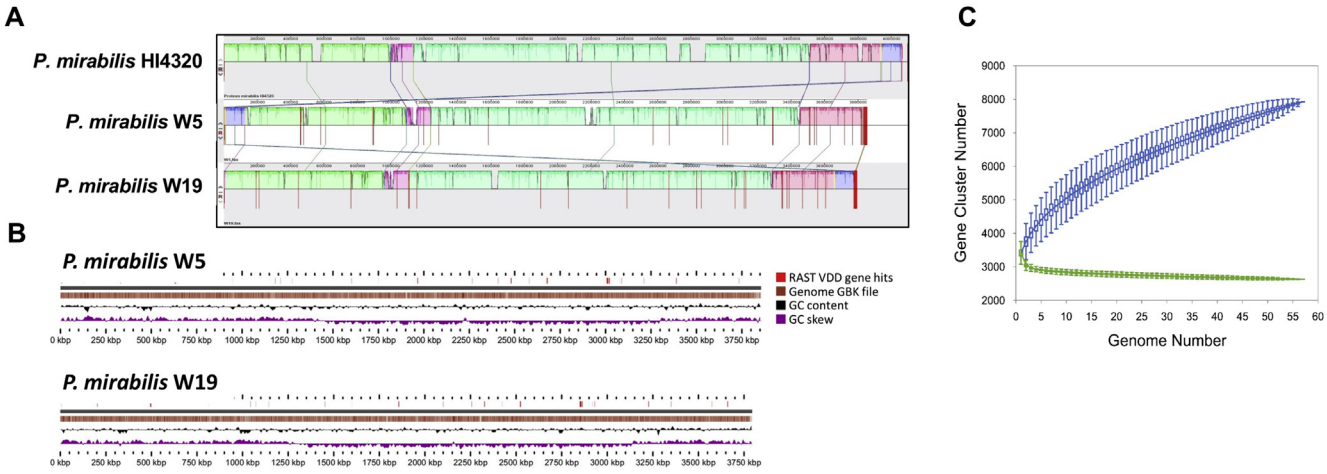

Supplementary Figure 3. (*A*) Mauve alignment of National Center for Biotechnology Information (NCBI) reference genome *P mirabilis* HI4320, with the genomes of *P mirabilis* strains W5 and W19. There is an extensive degree of gene synteny shared among all 3 genomes and with minimal rearrangements. (*B*) Linear representations of the genomes of *P mirabilis* W5 and W19 showing the location of their respective genes assigned to the Virulence, Disease and Defence (VDD) category by RAST annotation pipeline and visualized using Gview, as described in the Materials and Methods. The gene count is slightly larger in strain W5 (n = 37) compared with W19 (n = 35). (*C*) Core and pan-genome plots derived from the 57 *P mirabilis* genomes representing the 24 clinical isolates from Hong Kong patients with CD and the 33 additional *P mirabilis* genomes deposited in the NCBI databases. The plots are visualized using the PANGP tool with the core-genome size model shown in *green* ($893.59 \times 57^{0.44} + 2554.75$) and the pan-genome model shown in blue ($531.26 \times e^{-0.1 \times 57} + 2677.6$).

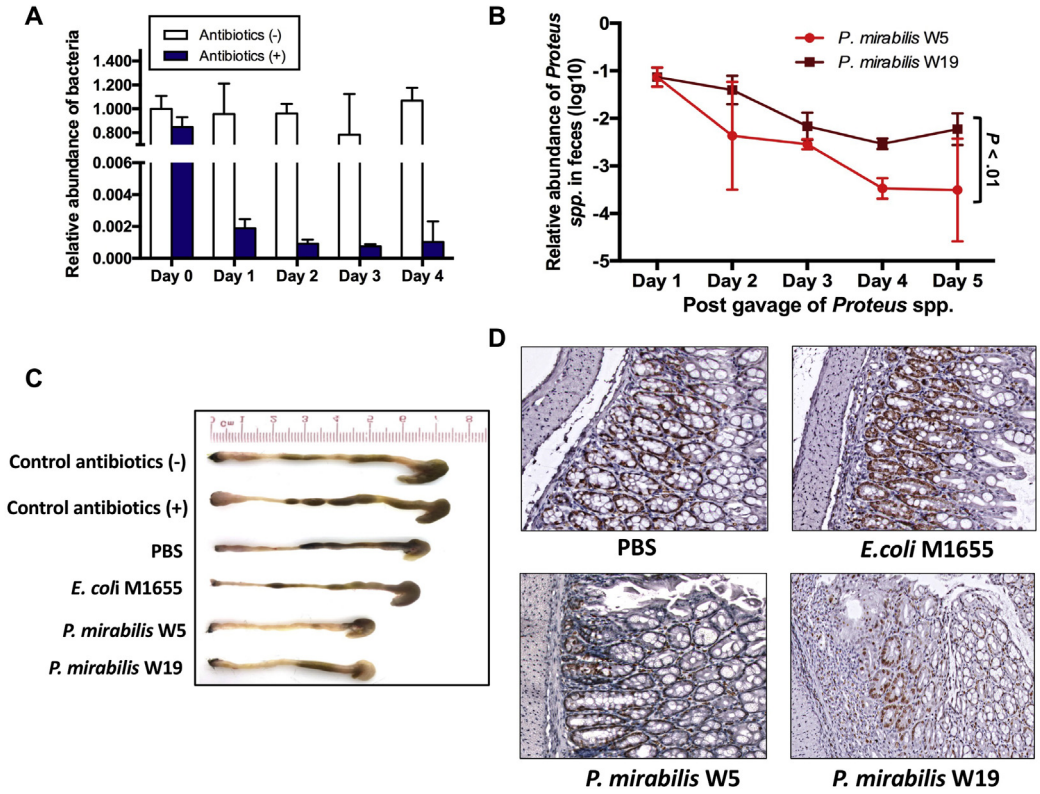

Supplementary Figure 4. (*A*) The level of total bacteria in stool samples of mice was determined by qPCR. (*B*) The level of *P mirabilis* in stool samples of mice post *P mirabilis* feeding was determined by real-time qPCR. (*C*) Representative colonic morphologies of mice under different treatment. (*D*) Cell proliferation in inflammatory and normal tissues isolated from *P mirabilis* inoculated or control mice was determined by Ki-67 staining. Cell proliferation index was quantified by counting the proportion of Ki-67–positive cells.

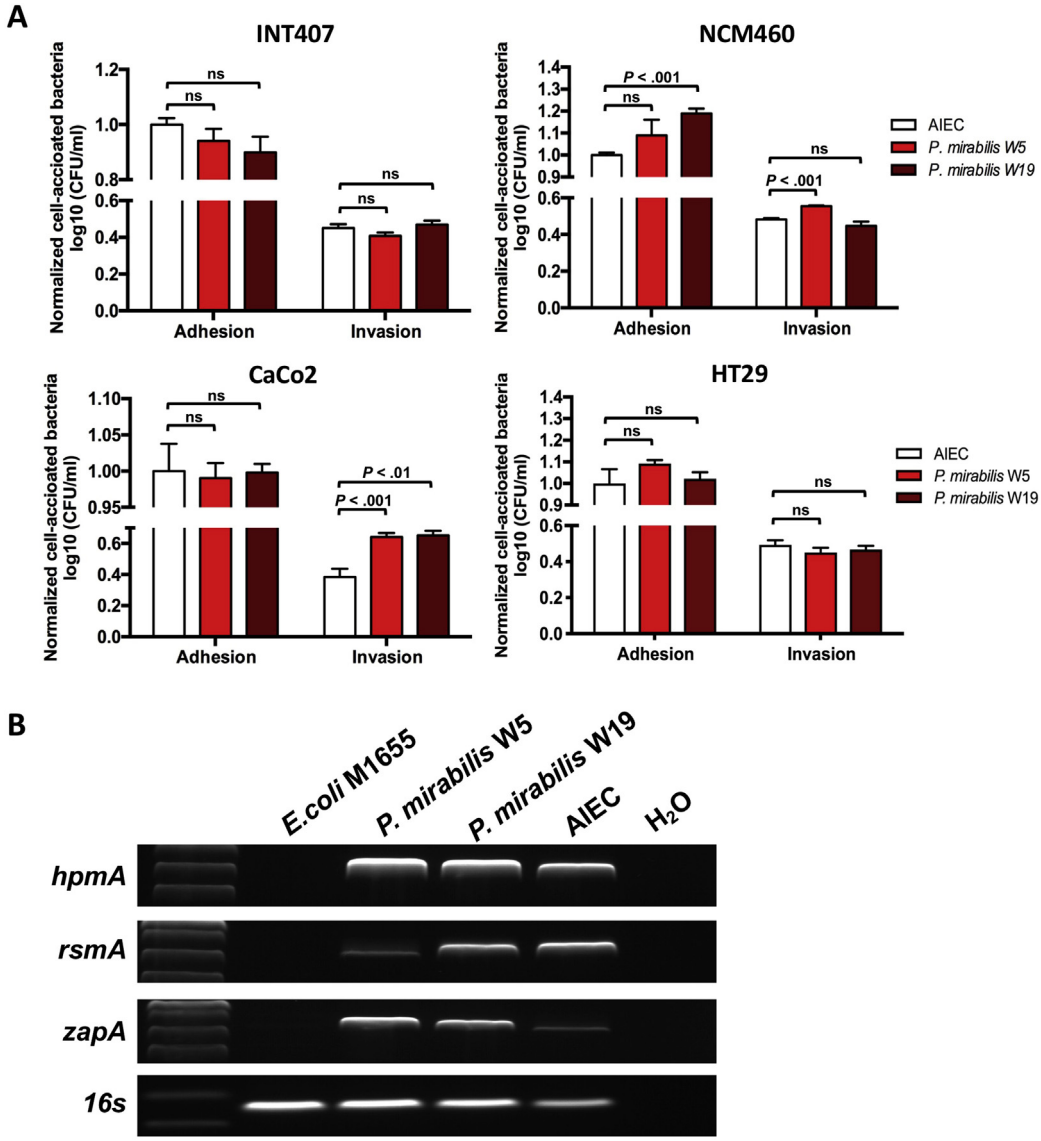

Supplementary Figure 5. (*A*) Adhesion and invasion assays performed on INT407, NCM460, CaCo2, and HT29 cells infected with adherent invasive *E coli* (AIEC), *P mirabilis* W5 and W19. Adhesive and invasive percentage of *P mirabilis* was compared with AIEC. Values are mean of 3 independent experiments. *Error bars* indicate SDs. One-way analysis of variance was performed for statistical significance. (*B*) Expression of invasion-related genes in *E coli* M1655, AIEC, and *P mirabilis* strain W5 and W9.

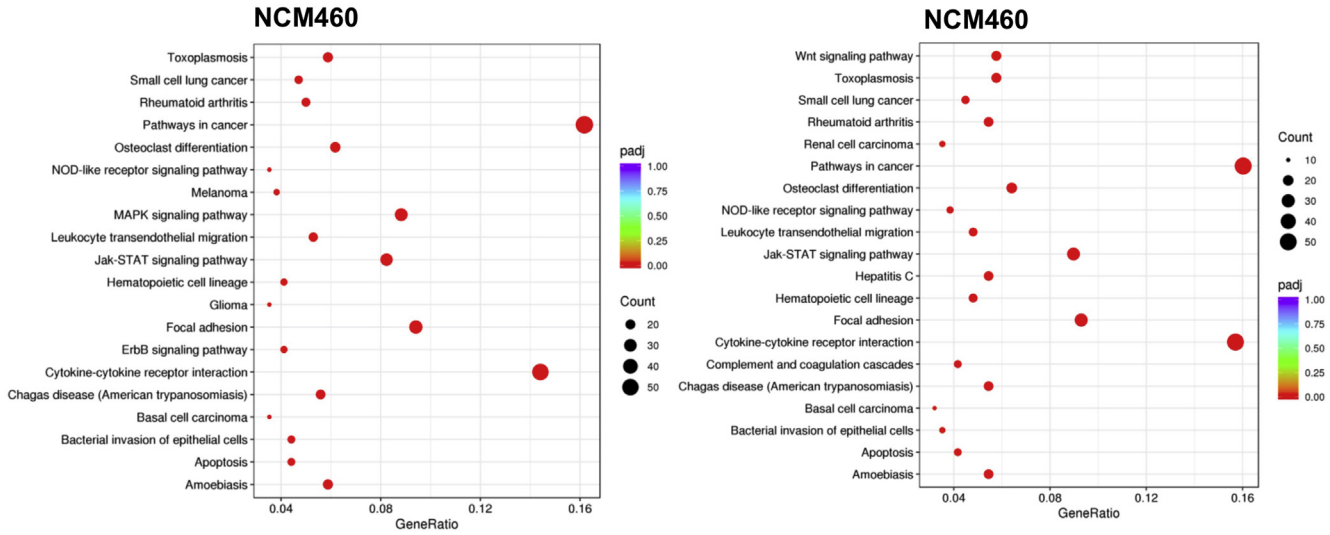

Control vs *P. mirabilis* W5 **Control vs *P. mirabilis* W19**

Supplementary Figure 6. Enriched signaling pathways modulated in response to the *P mirabilis* strains in NCM460 cells by KEGG pathway analysis.

Supplementary Table 1. Clinical and Pathologic Characteristics of Patients

Characteristic	Abundance of *Proteus* spp	
	High (n = 24)	Low (n = 43)
Age, *y*, mean ± SD	43.4 ± 11.5	44.7 ± 15.85
Sex, n (%)		
Male	16 (66.7)	27 (62.8)
Female	8 (33.3)	16 (37.2)
Abnormal pain, n (%)		
None	18 (75)	28 (65.1)
Mild	5 (20.8)	13 (30.2)
Moderate	2 (8.3)	1 (2.3)
Severe	1 (4.2)	1 (2.3)
Well-being, n (%)		
Well	10 (41.7)	25 (58.1)
Slight under par	11 (45.8)	12 (27.9)
Poor	2 (8.3)	2 (4.7)
Very poor	1 (4.2)	4 (9.3)
Anti-diarrhea drug use, n (%)		
Yes	3 (12.5)	0 (0)
No	21 (87.5)	43 (100)
Extraintestinal findings/ complications, n (%)		
Yes	11 (45.8)	9 (20.9)
No	13 (54.2)	34 (79.1)

Supplementary Table 2. Clinical Characteristics of the Included Patients With Crohn's Disease

Clinical characteristics	All patients (n = 67)
Age at diagnosis of Crohn's, *y*, median (IQR)	42.81 (30–53)
History of smoking at diagnosis (current/ former smokers), n (%)	14 (20.9)
Disease duration, *y*, median (IQR)	10.45 (4.808–16.09)
Montreal Classification (location), n (%)	
L1 (ileal)	0 (0)
L2 (colonic)	24 (35.8)
L3 (ileocolonic)	43 (64.2)
L4 (upper gastrointestinal involvement)	2 (3.0)
Perianal involvement, n (%)	11 (16.4)
Montreal Classification (behavior), n (%)	
B1 (non-stricturing, non-penetrating)	43 (64.2)
B2 (stricturing)	13 (19.4)
B3 (penetrating)	17 (25.4)
History of previous bowel resection, n (%)	12 (17.9)
Medications used at the time of study recruitment, n (%)	
Immunosuppressants	37 (55.2)
Prednisolone	5 (7.5)
Infliximab	18 (26.9)
Adalimumab	8 (11.9)
Antibiotic use within 3 mo, n (%)	10 (14.9)

NOTE. Percentages were based on non-missing data.
IQR, interquartile range.

Supplementary Table 7. The Expression of Up-Regulated Proinflammatory Genes, Which Shared Between *Proteus mirabilia* Strain W5 and W19 Administrated Germ-Free Mice

Gene	Full name	Fold-change	
		P mirabilis W5	*P mirabilis* W19
Ccl11	Chemokine (C-C motif) ligand 11	2.730884853	2.73088485
Ccl12	Chemokine (C-C motif) ligand 12	2.617377016	10.15717367
Ccl5	Chemokine (C-C motif) ligand 5	1.528664026	1.612386423
Ccr3	Chemokine (C-C motif) receptor 3	1.785805774	1.921016267
Cxcl11	Chemokine (C-X-C motif) ligand 11	3.317870865	6.178057921
Cxcl5	Chemokine (C-X-C motif) ligand 5	23.70393102	63.12129309
Cxcr1	Chemokine (C-X-C motif) receptor 1	2.565974912	1.885089207
Cxcr2	Chemokine (C-X-C motif) receptor 2	8.063067226	8.84332794
Fos	Fos Proto-Oncogene	5.288662712	5.696826776
Il18	Interleukin 18	2.280207788	7.913060369
Il1a	Interleukin 1 Alpha	1.815803181	4.769050844
Il1rn	Interleukin 1 Receptor Antagonist	3.525576628	2.246276902
il23r	Interleukin 23 receptor	2.592329875	1.918559386
Il6ra	Interleukin-6 receptor subunit Alpha	2.800044258	4.413449647
Myd88	Myeloid Differentiation Primary Response 88	2.7202447	1.719130606
Nfkb1	Nuclear Factor Kappa B Subunit 1	2.713	1.509501658
Ptgs2	Prostaglandin-Endoperoxide Synthase 2	3.470105164	12.14678681
Ripk2	Receptor Interacting Serine/Threonine Kinase 2	2.212167882	6.059518292
Tlr7	Toll-like receptor 7	2.227318645	9.484809647
Tnf	Tumor necrosis factor	8.033	6.770198822
Tnfsf14	Tumor necrosis factor (ligand) superfamily, member 14	1.81087845	2.731327152